ORIGINAL PAPER

Construction and use of rock-cut cisterns: a chronological OSL approach in the arid Negev Highlands, Israel

Andrea Junge[1] · Zachary C. Dunseth[2] · Ruth Shahack-Gross[3] · Israel Finkelstein[4] · Markus Fuchs[1]

Abstract

The Negev Highlands (Israel) are characterized by a rich settlement history over the last millennia. To sustain life in this arid environment, measures to collect and store water were introduced. Two types of installations to collect and store runoff water were built in the region: open reservoirs, and more elaborate subterranean rock-cut cisterns. This article focuses on the latter. Based on a few inscriptions found in rock-cut cisterns, it is assumed that the majority were constructed in the Hellenistic (Nabatean) to Byzantine period. To evaluate this age assessment, this study was carried out at the Borot Hazaz cisterns system, using optically stimulated luminescence (OSL) dating together with micromorphological analyses. Both were applied to sediments that were relocated during the cistern's construction and usage and after the maintenance activities ended. Despite unfavourable conditions for resetting the OSL signal, including fluvial transport over short distances and sediment deposition by humans in large quantities, it was possible to reconstruct the life cycle of the cistern system. The present study places the construction of the system during the late Roman to Byzantine period, with utilization and long-term maintenance during the following centuries. Maintenance ceased at the Borot Hazaz cistern system gradually over the course of the last 500 years.

Introduction

The arid Negev Highlands in southern Israel feature stone-built archaeological evidence for human activity in several periods—the Early Bronze and Intermediate Bronze Ages (ca. 3500–2000 BCE), the late Iron I–Iron IIA (ca. 1000–800 BCE) and the Hellenistic-Roman-Byzantine and

Ruth Shahack-Gross, Israel Finkelstein, Markus Fuchs are Project directors

✉ Andrea Junge
andrea.junge@geogr.uni-giessen.de

1 Department of Geography, Justus Liebig University Giessen, Senckenberstr. 1, 35390 Giessen, Germany

2 Joukowsky Institute for Archaeology and the Ancient World, Brown University, Providence, RI, USA

3 Department of Maritime Civilizations, Charney School of Marine Sciences, Recanati Institute of Maritime Studies, University of Haifa, Haifa, Israel

4 Institute of Archaeology, Tel Aviv University, Tel Aviv, Israel

Early Islamic periods (ca. 200 BCE–800 CE, although in this phase both the beginning and end are disputed). Stable water sources in this region are few and their yield is rather low. Hence, during certain periods of strong human activity, hundreds of open-water reservoirs and subterranean cisterns (Fig. 1) were constructed to collect runoff water during the scarce rain events (Evenari et al. 1982; Rubin 1988).

The simpler open reservoirs (Fig. 1a) are man-made basins located along footslopes dug into soft sediments and lined with stones in order to stabilize them (Evenari et al. 1958; Rubin 1988). They have no protective roof, leading to contamination and significant water loss due to evaporation. The permeable soft sediments result in water loss through infiltration. The subterranean cisterns (Fig. 1b) are less vulnerable to pollutants, and the protective roof limits evaporation even during the hot and dry summer months. These installations were usually hewn into less-permeable solid chalk formations, and occasionally lined with plaster (Evenari et al. 1958).

In terms of construction and maintenance, the two types of water storage systems are similar. During construction,

Fig. 1 Photographs of **a** the open water reservoir of Bor Hemet (16–18 m wide) and **b** cistern III of the Borot Hazaz system. Both have been maintained recently for tourism.

the excavated material (sediment or chalk) was deposited on a spoil pile close to the installation. To increase their water catchment area, dams and channels were built on the adjacent slopes to direct the surface runoff into the cistern or reservoir (Figs. 2 and 3). However, surface runoff also fed the water storage systems with sediments eroded from the catchment. While the systems were in use, these sediments needed to be occasionally removed from the installations, and were deposited on the adjacent spoil piles. With the cessation of maintenance, the reservoirs and cisterns were rapidly refilled by sediments.

While the construction and operating principles of open-water reservoirs and subterranean cisterns are similar, the chronology of the two types of installations, and the relationship between them, is not clear. Open reservoirs are traditionally dated to the Iron Age based on their proximity to sites from this period (e.g., Cohen & Cohen-Amin 2004; Evenari et al. 1958; Haiman 1991; Lender 1990). A recent study by Ore et al. (2020) showed a spatial correlation between open reservoirs and Early Bronze Age and/or Intermediate Bronze Age sites. Based on this circumstantial

evidence, the authors placed the construction of open reservoirs predominantly during these periods. Focusing on sites with chronometric data, Junge et al. (2018) used optically stimulated luminescence (OSL) to determine the age of an open reservoir near the site of Atar Haroa and present a detailed history of the reservoir. Micromorphology was used to identify different modes of deposition, and consequently support the interpretation of the OSL ages. This research indicated the open reservoir was constructed in the eighth–eleventh century CE (the Early Islamic period), and continued to be utilized and maintained until the fifteenth century CE (medieval period), and subsequently infilled with sediment due to cessation of maintenance. These results showed that while the habitation site of Atar Haroa dates to the Iron Age IIA (mainly ninth century BCE; Boaretto et al. 2010), the reservoir next to it is not contemporaneous, highlighting the difficulty in determining ages of spatially close yet disconnected archaeological features.

In contrast to open-water reservoirs, the construction of rock-cut cisterns in the Negev Highlands is traditionally constrained between 200 BCE and 640 CE based on Nabatean and Byzantine inscriptions discovered on the walls of several of these installations (Rubin 1988). Tepper et al. (2020) attempted to use OSL dating to determine the age of a rock-cut cistern that is part of an agricultural system near the ancient (mainly Byzantine) village of Shivta. The spoil pile related to it was dated to the sixteenth century CE, and was interpreted as representing the maintenance of the cistern. In comparison, the shallow sediment accumulation within the cistern was dated to 60 ± 10 years old, representing the time after the last cleaning of the cistern. No spoil pile containing construction material was included in this study, and therefore the cistern's construction could not be determined by numerical dating.

To evaluate the archaeological age of the subterranean cisterns based on typology, inscriptions and artefacts, it is necessary to apply numerical dating on sediments that are not only associated with the construction of cisterns, but also with the utilization and maintenance of these installations. In the current study, OSL dating was used at the elaborate system of cisterns known as Borot Hazaz, located ca. 5 km to the northeast of Kibbutz Sede Boqer (Fig. 2). The study aims to determine sediment deposition of the following stages: (1) construction (rock-cutting), (2) maintenance and (3) cessation of maintenance of the cisterns.

To support the interpretation of the OSL results and to identify the mode of sediment deposition, detailed micromorphological analyses were conducted in tandem. A complete chronological life cycle of the Borot Hazaz cisterns is presented for the first time, and the methodological approach can be used as a general blueprint for establishing cistern chronologies.
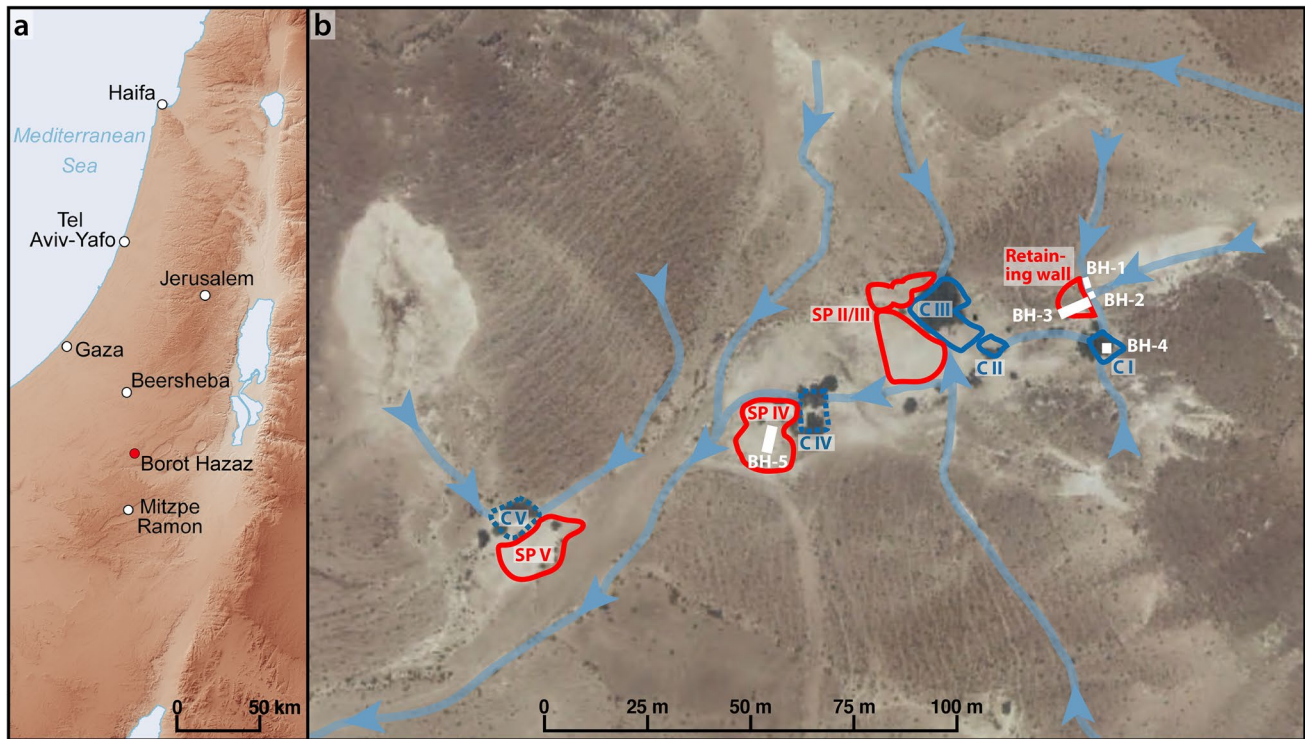
Fig. 2 a Map of the southern Levant with the location of the Borot Hazaz cistern system marked in comparison to modern cities, and **b** satellite image of the study area (Survey of Israel 2007). The position and layout of the cisterns are marked in dark blue (dotted lines indicate that the size of the cistern cannot be estimated due to complete infilling) and the locations of the spoil piles are marked in red. The light blue lines show the channels that conduct the water from the slopes to the cisterns, and from one overflowing cistern to the next. When the cisterns are completely filled, water exits the system following the wadi's depression line out of the system to the southwest. The arrows indicate the direction of water flow. The white boxes indicate the location of the excavated trenches.

The study area

The arid Negev Highlands are situated in the south of modern Israel, with elevations ranging between 600 m a.s.l. in the northeast and 1000 m a.s.l. in the southwest (Fig. 2a). The rolling-hill topography was formed following the uplift of the highlands and faulting processes of the Dead Sea Rift during the Late Miocene to the Early Pleistocene, resulting in a series of northeast-to-southwest-oriented anticlines and synclines (Avni et al. 2006; Itzhaki 1971). The bedrock mainly consists of Cretaceous and Eocene marine carbonates (primarily limestone, dolomite, chalk, chert and marl), traversed by wadis, which are the result of erosion processes during the Plio-Pleistocene (Avni & Weiler 2013; Bruins 1986; Starinsky et al. 2010). Aeolian sediments primarily from the Sinai and the Sahara accumulated across the Negev Highlands during the Late Pleistocene and Early Holocene (Avni et al. 2012, 2006; Crouvi et al. 2008; Roskin et al. 2011). Following this, the formation of thick alluvial deposits in the wadis was caused by erosion of aeolian fines and mixing with local sediments (Avni et al. 2013; Bowman et al. 1986; Faershtein et al. 2016). These sediments are found redeposited as the accumulations within the cisterns and channels, as well as in the maintenance accumulations on the spoil piles.

The present-day climate in the study area is characterized by mean annual air temperature between 17 and 19 °C (with temperatures in the summers up to 40 °C, and winters down 0 °C) and annual precipitation between 80 and 150 mm (Kafle & Bruins 2009). Most rainfall occurs during the winter months, roughly between October and April (Avni et al. 2006; Goldreich 2003), with strong year-to-year variations (Bruins 2012; Evenari et al. 1982; Shanan 2000). Fog and dew add to the annual precipitation an equivalent of 10 mm for each 100-m increase in elevation (Kidron 1999).

In the study area, the climate of the last 2000 years is characterized by lower precipitation at the beginning of the first millennium CE compared to the following centuries and the modern climate (Bar-Matthews & Ayalon 2004; Orland et al. 2009; Bookman et al. 2004; Neumann et al. 2010). Bar-Matthews et al. (2003) reconstructed drier conditions during most of the last two millennia, while Neumann et al. (2010) and Bookman et al. (2004) postulated strong oscillations in precipitation following an initial reduction at the beginning of the first millennium CE. Orland et al. (2009) described a second decrease in rainfall at about 400 CE,
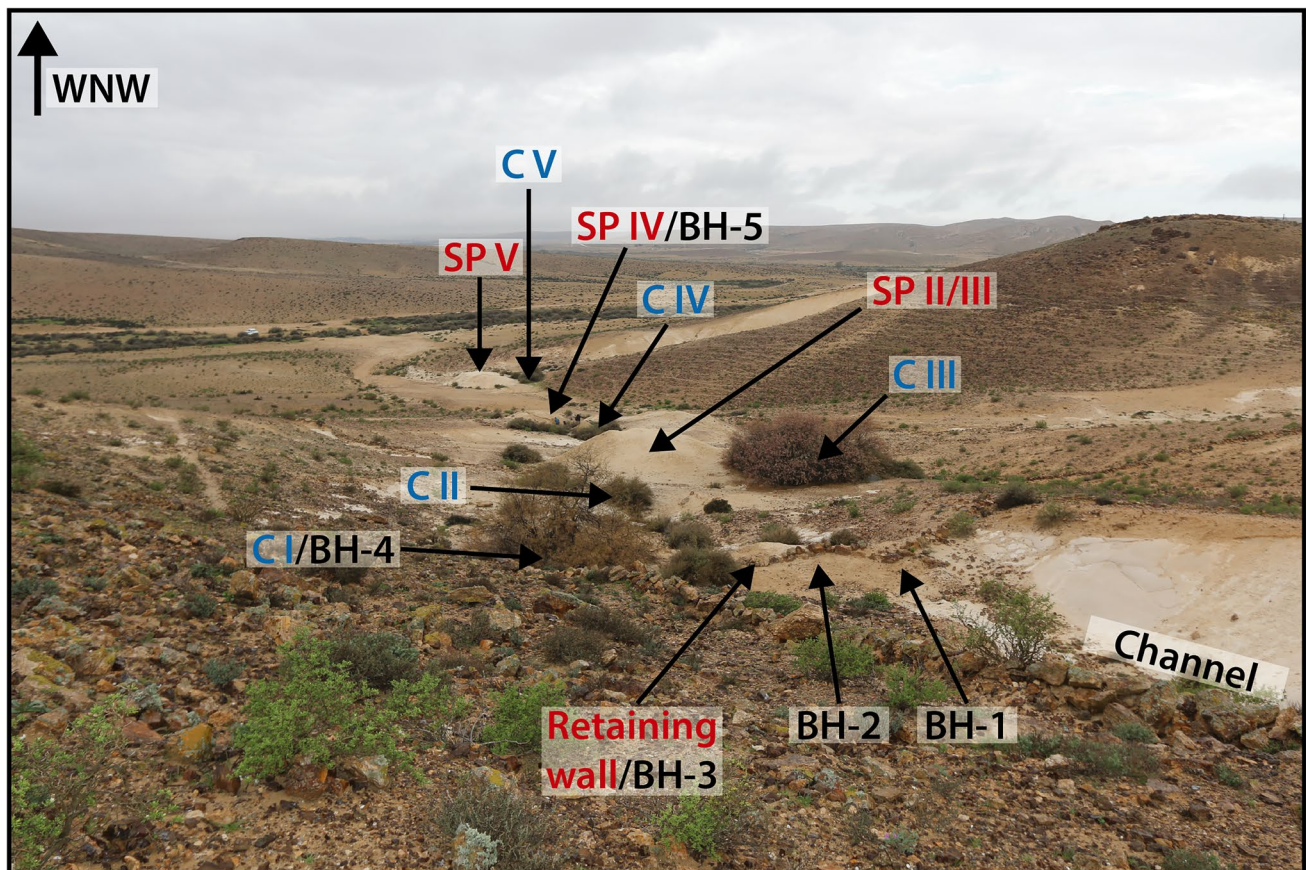
Fig. 3 Overview photograph of the Borot Hazaz cistern system. The location of the cisterns (C) I–IV are marked in blue, the spoil piles (SP) II-IV and the retaining wall of cistern I in red, and the excavated trenches BH-1 to BH-5 are marked in black.

possibly followed by further variations, which follows other palaeoclimate reconstructions presenting similar arid events between 500 and 1600 CE (Heim et al. 1997), or between 500 and 1200 CE (Migowski et al. 2006).

Although these climate reconstructions do not show a congruent picture of the changes in precipitation over the last 2000 years, they generally indicate drier or similar conditions compared to today's precipitation regime in the study area.

The cisterns system

The installations studied here belong to the water harvesting system of Borot Hazaz (cisterns), located in the northern part of the Negev Highlands (Fig. 2a) within a small wadi that drains from the northeast to southwest into Nahal Hazaz (Fig. 2b). During sufficiently strong precipitation events, the adjoining slopes to the north, east and southeast feed the cisterns with surface runoff. The system consists of five subterranean cisterns of different sizes, several channels that lead surface runoff from the slopes into the cisterns, and

spoil piles with sediments from the construction and maintenance of the installations. The cisterns were dug into the soft chalk of the Menuha Formation (Avni & Weiler 2013). The arrangement of the cisterns follows the direction of the wadi from cistern I in the northeast to cistern V in the southwest (Figs. 2b and 3).

The cisterns are rectangular in shape and show no evidence for plastering, which was done in some cisterns to reduce the permeability of the chalk they are cut into. Due to its large size of ca. 15 m by 9 m, cistern III has two roof-supporting rock-cut pillars aimed to stabilize the overlying bedrock. Because cisterns I and II are only ca. 3 by 4 m, pillars did not appear to be necessary to support the roof in antiquity, although parts of the roof of cistern I have since collapsed. Cisterns IV and V are completely filled with sediments, and consequently, determining their size and shape is impossible without excavation. Since none of the cisterns was completely excavated during this study, their water capacity can only be approximated and ranges in the order of dozens of cubic metres to several hundred cubic metres.

The Borot Hazaz cistern system is described by Cohen (1981) but no excavations or detailed analyses were

conducted at that time. According to a local farmer, the largest cistern in the system (cistern III) was cleaned in the 1960s by members of a nearby kibbutz to water their flocks.

Sampling strategy

The investigations focused on cistern I along with its channel, retaining wall and its sediment fill, as well as on the spoil pile of cistern IV (Figs. 2b and 3). The time of construction, utilization and cessation of maintenance of these cisterns was determined by OSL dating of the different components of the system, while micromorphological analyses were used to identify the different modes of sediment deposition. The infill of cistern I was selected for excavation since no recent use or disturbance was visible on the surface, and because it was easily accessible.

The channel of cistern I: trench BH-1 and BH-2

The sediment accumulation in the channel leading water into cistern I was excavated and sampled in two locations (Figs. 2b and 3, BH-1 and BH-2). The base of both trenches was the chalk bedrock of the Menuha Formation (Fig. 4). The sediments exposed in these trenches were composed of layered fluvial fines and stony debris of up to 10 cm in diameter. Evidently, sedimentation within the channel took place after the last channel cleaning. To evaluate when maintenance and cleaning activities ceased, two OSL samples were taken from the section in the western trench (BH-1, Fig. 4b) and three OSL samples from the section in the eastern trench (BH-2, Fig. 4a). The samples at the base of both sections date the onset of the final sediment accumulation within the channel. The sampling of the overlying sediments was carried out to gather information about the development of sediment accumulation in the channel.

The retaining wall of cistern I: trench BH-3

A retaining wall was constructed to redirect surface runoff from the channels into cistern I (Figs. 2 and 3). It is assumed that the cistern could only be used while the retaining wall existed; otherwise, only a fraction of the available surface runoff would reach the cistern. Thus, by dating the construction of the retaining wall, a temporal connection to the cistern's construction can be established. The retaining wall was cut at some point by water overflowing from the cistern. This existing cut was trenched from the channel-facing part of the retaining wall to its lower limit (Fig. 5, BH-3). The bottom of the trench was defined by bedrock and
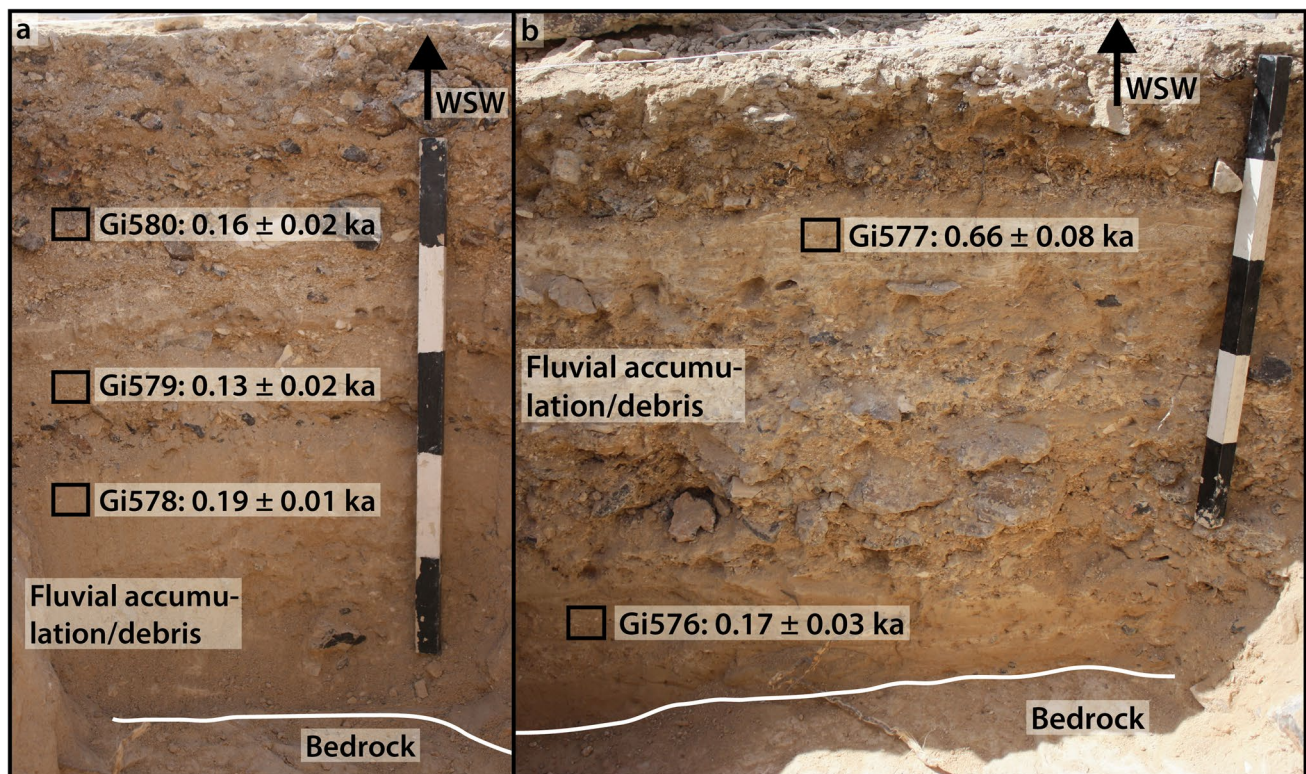
Fig. 4 Trench BH-2 (**a**) and BH-1 (**b**) showing the sediment accumulation and bedrock within the channel leading towards cistern I. Location of the OSL samples are marked by black boxes and labelled and the ages are presented. One unit of the scale bar equals 10 cm.
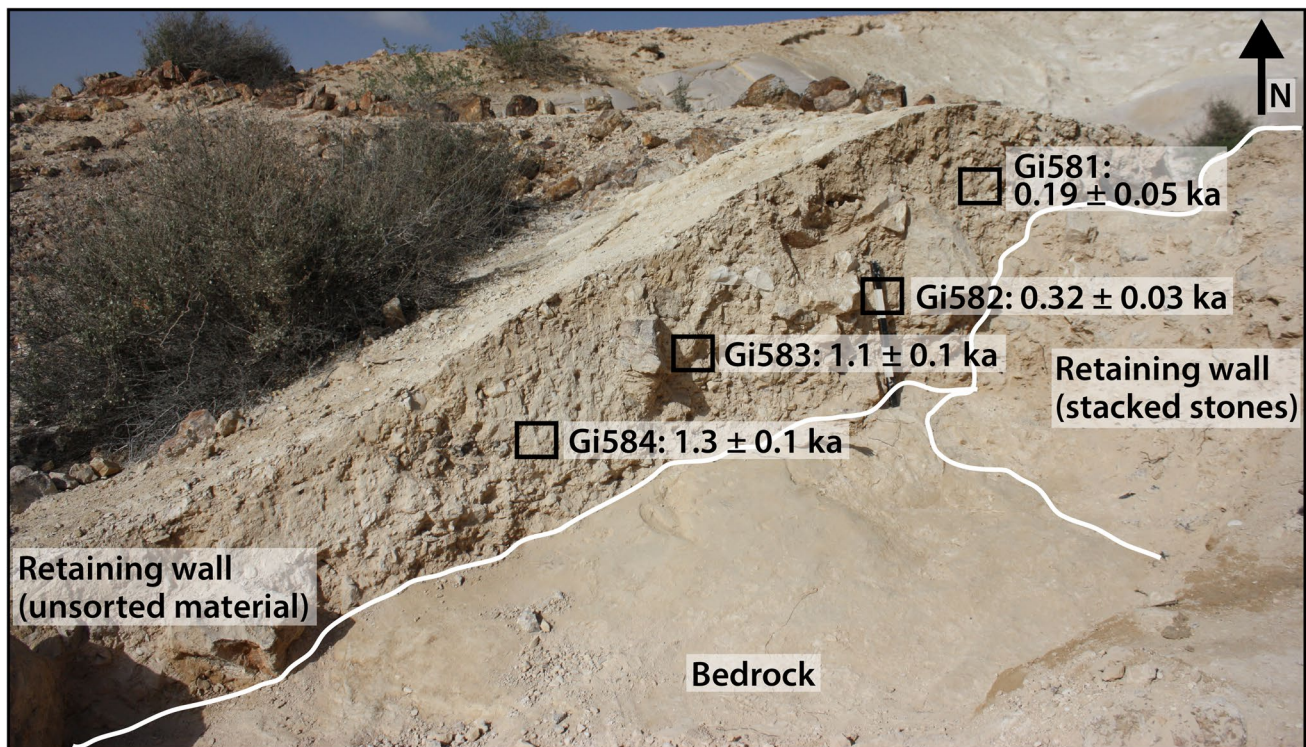
Fig. 5 Trench BH-3 cuts through the retaining wall of cistern I. Location of the OSL samples are marked by black boxes, the samples are labelled and ages presented.

the channel-facing end of the retaining wall was constructed of flat limestone slabs. On top of the stacked stones, and in the centre and lower end of the trench, sediments and stones were exposed, likely deposited to stabilize the feature. This deposit showed no layering or orientation, and consequently only one depositional event can be identified by stratigraphic evidence. To determine if more than one event was exposed, and to constrain the time of construction and possible maintenance event(s), four OSL samples were taken across the exposed section (Fig. 5).

Filling of cistern I: trench BH-4

The sediments within cistern I (Figs. 2b and 3) were interpreted as the accumulation after the last cleaning of the installation. They were composed of fluvial fines with vague layering (Fig. 6, BH-4). The trench was cut 2 m deep without reaching bedrock. The accumulation was mixed with plastic and metal trash. Three OSL samples were taken, but only the lowermost sample was prepared and measured to check the reliability of the OSL dating approach for the cistern filling, as it could be correlated with a (pre)modern enamelled metal bucket found next to the OSL sampling location. At the same depth, a micromorphology sample was taken in order to identify the mode of sediment deposition at the bottom of the trench.

The interpretation of OSL ages from cistern I is limited, because the contemporaneity of the construction of the cistern and the retaining wall is only assumed, and a spoil pile with a clear succession of construction and maintenance material was not available to sample. Therefore, the spoil pile of cistern IV (Figs. 2 and 3) of the system was added to the study.

The spoil pile of cistern IV: trench BH-5

The spoil pile of cistern IV (Figs. 2 and 3) was cut in the past by water overflow from the cistern. A four-step trench was excavated in the original centre of the spoil pile (BH-5, Fig. 7) to expose the complete stratigraphy, as well as conserve the spoil pile. The lowermost and the uppermost steps were sampled and studied in detail. At the bottom of the lower step, the chalk bedrock was exposed, overlain by unsorted alluvial sediments that accumulated before cistern IV was constructed. Above this palaeosurface, construction and maintenance material were deposited. The top step of the trench was composed of three layers of construction and maintenance material. Both steps were sampled in triplicate for OSL dating to constrain pre-construction, construction and maintenance over time. One micromorphology block encompassing the contact between the pre-construction and construction
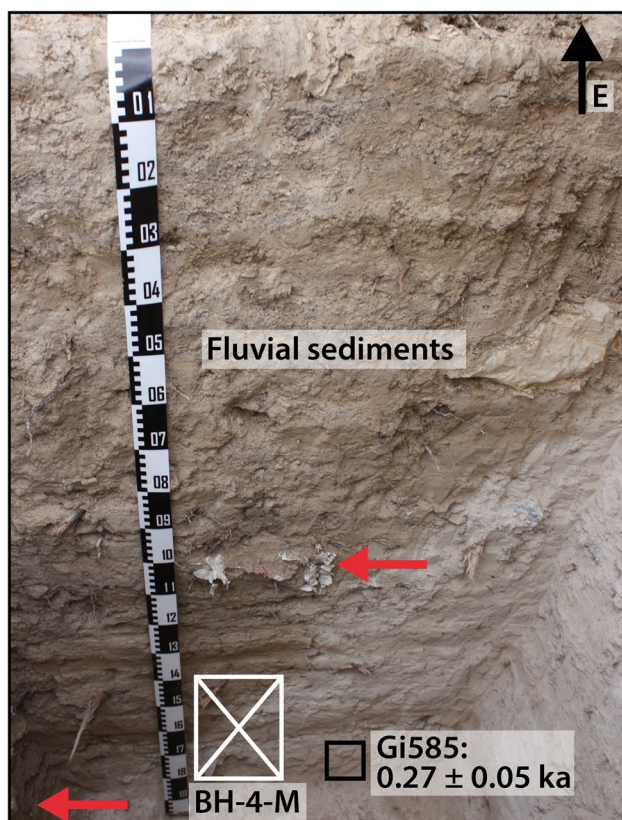
Fig. 6 Trench BH-4, situated within cistern I. Location of the OSL sample is marked by a black box, the sample number is labelled and the age presented. A micromorphology sample (BH-4-M, white box) was taken from the bottom of the eastern section. The upper arrow points at a plastic item and the lower arrow points at an enamelled metal bucket. The small graduation on the left side of the scale bar equals 1 cm, the units on the right represent 10 cm.

deposits was collected to confirm the presumed modes of deposition.

Methods

Optically stimulated luminescence dating

The majority of OSL samples were collected at night by thoroughly cleaning the sections before OSL sampling and filling the sample material directly into light-proof bags. Two of the analysed OSL samples (Gi577 and Gi585) were sampled during daytime using steel cylinders with a diameter of 5.6 cm. To determine the equivalent dose (D_e), the coarse-grain (90–200 μm) quartz fraction was prepared. First, sediment was removed from the bags or cylinders, and in the latter case the bleached material at both ends of the cylinders was discarded. The sediment was wet-sieved to separate the grain-size fractions, followed by treatment with 10% HCl and 10% H_2O_2 to dissolve carbonates and oxidize organic matter. To obtain the quartz fraction, lithium-heteropolytungstate (2.63 and 2.68 g/cm^3) was used for density separations. Next, the quartz extract was etched in 40% hydrofluoric acid (HF) for 80 min to remove the α-irradiated outer rim of the grains and to eliminate any remaining feldspar contamination. Finally, the coarse-grain quartz fraction was washed for 30 min in 10% HCl and re-sieved (63 μm) to remove small residues and remaining feldspar fragments. All sample preparation was performed under subdued amber-coloured light centred on a wavelength of 590 ± 10 nm.

The OSL measurements were executed on a Lexsyg Standard reader (Lomax et al. 2014). For stimulation, the reader was operated with green LEDs (525 ± 25 nm), whereas for signal detection, a Hamamatsu H7360 photomultiplier combined with a 5-mm Semrock HC377/50 filter and a 3-mm Schott BG3 filter was applied. This combination restricts the detection window to ca. 350–400 nm, thus is centred on the main OSL emission of quartz (Huntley et al. 1991; Lomax et al. 2015). Stimulation with infrared (IR) laser diodes (850 ± 3 nm) was used to check for the purity of the quartz extracts. Feldspar contamination was tested by applying the OSL IR depletion ratio (Duller 2003). For this test, IR signals were detected through a 3.5-mm Semrock HC414/46 interference filter in combination with a 3-mm Schott BG39 filter, which restricts the detection window to ca. 395–430 nm. Sample irradiation was performed with a calibrated 90Y/90Sr β-source (1.8 GBq), resulting in a dose rate for coarse-grain quartz on stainless steel cups of 0.119 ± 0.003 Gy/s (February 2019).

For the determination of D_e, a single-aliquot regenerative-dose (SAR) protocol was applied (after Murray and Wintle 2000, 2003). To define the dose–response curve, five or six regeneration cycles, including the zero dose and one repeated dose point, were used. The shine-down curves were measured for 50 s at elevated temperatures (125 °C) after a preheat at 180 °C (10 s) and a cut-heat at 160 °C for the natural and regenerated signals. The preheat and cut-heat temperatures were chosen after combined preheat-dose recovery tests (DRT, Fig. 8a) and preheat-plateau test (PHT, Fig. 8b) for the two samples representing construction (Gi592) and maintenance (Gi593) material. For the DRT, the samples were bleached in the Lexsyg reader using the green LEDs and irradiated with a known β-dose close to the natural dose, followed by D_e determinations using a SAR protocol. For the PHT, burial doses were also measured using the SAR protocol. Both tests were conducted at six different preheat temperatures (180–280 °C) with a cut-heat temperature 20 °C below the preheat temperature, but with a maximum at 220 °C. The tests were conducted on three fresh aliquots per temperature combination for each sample. The selection of the preheat (180 °C) and cut-heat (160 °C) temperatures used in this study is based on the successful replication of the known given dose within the 10% error range at 180 °C for
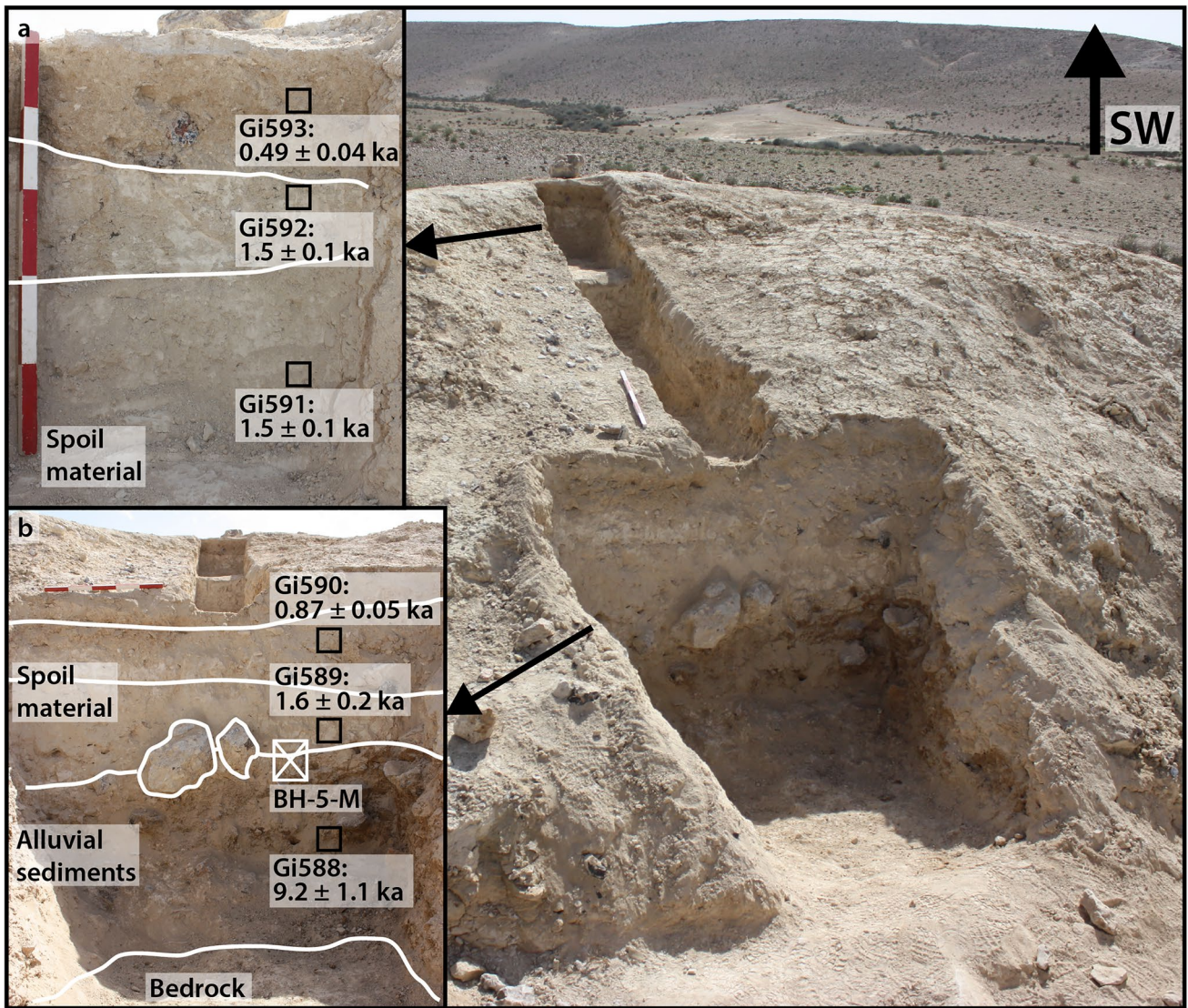
Fig. 7 Stepped trench BH-5 was cut into the spoil pile of cistern IV. The upper (**a**) and lower (**b**) steps of the trench were sampled and studied in detail. Location of the OSL samples are marked by black boxes, the samples are labelled and the ages presented. A micromor-phology sample (BH-5-M, white box) included the contact between the natural alluvial deposits and cistern construction material. One unit of the scale bar equals 10 cm.

Fig. 8 Results of the dose recovery tests (**a**) and preheat plateau tests (**b**) of samples Gi592 representing the sampled construction material and Gi593 representing the maintenance and refill material at this site. For each temperature combination, the average of three measured aliquots were calculated and displayed. The given doses for the dose recovery tests were 0.9 Gy for sample Gi592 and 3.0 Gy for Gi593.
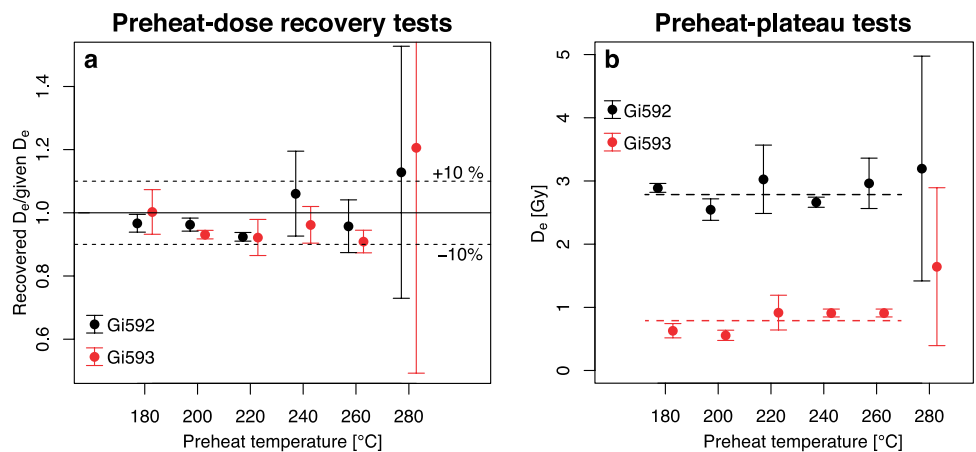
both samples using the DRT (Fig. 8a). The PHT supports this outcome by showing a preheat plateau covering the preheat temperatures from 180 to 260 °C (Fig. 8b).

For D_e calculation, the integral of the first 0.5 s of the quartz shine-down curves was used, after subtracting a background of 40 to 50 s from the signal. One- to 4-mm aliquots (30 to 500 grains; Burow 2020; Fuchs & Wagner 2003) were used for D_e determination of the coarse-grain fraction, depending on the amount of quartz material extracted and the strength of the OSL signal. In general, up to 60 aliquots were measured for each coarse-grain sample to determine the D_e. After passing the rejection criteria of 10% for the recycling ratio, the test dose error, the recuperation value and the OSL IR depletion ratio, and 15% for the palaeo-dose error, the mean D_e of the aliquots was calculated using the central age model after Galbraith et al. (1999) for not significantly skewed samples, and the bootstrap minimum age model (Cunningham & Wallinga 2012) for significantly skewed samples. The differentiation between skewed and un-skewed distributions is based on the comparison of the standardized values of skewness and their significance value (Bailey & Arnold 2006). The age models were calculated with log-transformed D_e values for samples with D_e values > 1 Gy (Gi584, Gi588, Gi591 and Gi592), whereas samples with measured D_e values ≤ 1 Gy (Gi576–Gi583, Gi585, Gi589, Gi590 and Gi593) were calculated based on the unlogged D_e (Arnold et al. 2009).

Radionuclide concentrations were determined by thick source α-counting (U and Th) and ICP-OES (K). To account for heterogeneous dose rate environments at the OSL sampling locations, dose rate samples were collected from the 30 cm surrounding the OSL sample, gathering material that represented the different sediments, stones and bedrock in the surroundings. The cosmic radiation dose was calculated according to Prescott and Hutton (1994). To estimate the change in attenuation of the cosmic dose rate over time, it is distinguished between a prompt and a gradual sediment accumulation: using current burial depths for the samples from the retaining wall (BH-3: Gi581–Gi584) and the spoil pile (BH-5: Gi588–Gi593), because the deposition interval of the material was relatively short and ended several centuries ago, and using half the current burial depths for the samples within the cistern (BH-4: Gi585) and within the channel (BH-1 and BH-2: Gi576–Gi580), because a relatively gradual accumulation continuing until the present day is assumed. The measured concentrations were converted to dose rates using the conversion factors of Guérin et al. (2011) and the β-attenuation factor of Mejdahl (1979). The age calculation was performed using DRAC v1.2 (Dose Rate and Age Calculator) by Durcan et al. (2015).

The water content for dose rate calculation was selected depending on which part of the cistern system the sample was collected from. The water content of the OSL sample collected within cistern I (BH-4: Gi585) was set to $15 \pm 7.5\%$. This value and its uncertainty represent the possible water content range based on the porosity of the loamy silt, the climatic conditions and the amount of water delivered by the channels from the adjacent slopes. The flood frequency in the channel is comparable to the situation inside of the cistern. However, unlike the cistern, the channel is not constructed to hold the water over longer periods of time. Taking this into account, the water content for the channel samples (BH-1 and BH-2: Gi576–Gi580) was set to $10 \pm 5\%$. For the retaining wall and spoil pile samples, a lower water content of $6 \pm 3\%$ is assumed because these structures are not fed by surface runoff from adjoining slopes, and they are better drained than both the cistern and the channel (Table 1). The actual measured water contents of the sediments after sampling confirmed the water content values utilized for the dose rate calculation. However, the water contents and their errors utilized were not solely based on the measured values, because they only represent the current hydrological conditions.

Micromorphology

The monolithic sediment blocks were extracted using plaster of Paris (gypsum) bandages. They were then dried at 50 °C for 3 days and impregnated by a 7:3 (v:v) mixture of polyester resin and acetone. A small amount of hardener (10 ml per 1 l of mixed resin) was added, without accelerator, in order to assure penetration of the resin into small pores before consolidation. After several weeks, the blocks were cured at 50 °C for 2 days and cut to the desired thin section size (5 × 7 cm) using a slab saw. Two thin sections, prepared by Quality Thin Sections (Arizona, USA), were yielded from each block, covering the length of the original sample. The final 30-µm thin sections were studied using a Nikon Eclipse 50i polarizing light microscope, in plane-polarized light (PPL) and crossed-polarized light (XPL) under various magnifications, and described using the conventional literature (Stoops 2003).

Results

Optically stimulated luminescence

As already shown in OSL dating studies at other archaeological sites in the Negev Highlands (e.g., Porat et al. 2006; Junge et al. 2016, 2018; Dunseth et al. 2017), the coarse-grained quartz is highly suitable for OSL dating. The quartz extract is characterized by a rapidly decaying OSL signal (Fig. 9) implying a prominent fast component of the OSL signal, resulting in bleaching even during short sunlight exposure (Bailey et al. 1997). A distinctive

Table 1 Sample ID, K-, Th- and U-content, cosmic dose rate, water content and the resulting dose rate (Ḋ).

Sample ID	K [%]	Th [ppm]	U [ppm]	Cosmic dose rate [Gy/ka]	Water content [%]	Ḋ [Gy/ka]
BH-1						
Gi576	0.43 ± 0.02	2.29 ± 0.63	5.15 ± 0.20	0.23 ± 0.02	10 ± 5	1.81 ± 0.08
Gi577	0.49 ± 0.03	1.51 ± 0.55	4.50 ± 0.18	0.28 ± 0.03	10 ± 5	1.66 ± 0.07
BH-2						
Gi578	0.34 ± 0.02	2.36 ± 0.78	6.66 ± 0.24	0.25 ± 0.03	10 ± 5	2.05 ± 0.09
Gi579	0.31 ± 0.02	1.30 ± 0.64	5.88 ± 0.20	0.26 ± 0.03	10 ± 5	1.79 ± 0.08
Gi580	0.24 ± 0.01	1.26 ± 0.49	6.17 ± 0.16	0.28 ± 0.03	10 ± 5	1.74 ± 0.07
BH-3						
Gi581	0.28 ± 0.01	1.28 ± 0.48	5.91 ± 0.15	0.23 ± 0.02	6 ± 3	1.85 ± 0.06
Gi582	0.31 ± 0.02	1.21 ± 0.46	5.74 ± 0.15	0.21 ± 0.02	6 ± 3	1.81 ± 0.06
Gi583	0.32 ± 0.02	1.67 ± 0.48	5.52 ± 0.15	0.23 ± 0.02	6 ± 3	1.82 ± 0.06
Gi584	0.36 ± 0.02	1.95 ± 0.57	4.87 ± 0.18	0.23 ± 0.02	6 ± 3	1.73 ± 0.06
BH-4						
Gi585	0.30 ± 0.02	2.00 ± 0.58	4.88 ± 0.18	0.20 ± 0.02	15 ± 7.5	1.52 ± 0.09
BH-5						
Gi588	0.91 ± 0.05	7.71 ± 0.82	3.52 ± 0.25	0.19 ± 0.02	6 ± 3	2.29 ± 0.09
Gi589	0.26 ± 0.01	3.64 ± 0.70	2.72 ± 0.22	0.20 ± 0.02	6 ± 3	1.26 ± 0.06
Gi590	0.30 ± 0.02	1.92 ± 0.65	4.52 ± 0.21	0.24 ± 0.02	6 ± 3	1.60 ± 0.06
Gi591	0.27 ± 0.01	1.35 ± 0.64	5.04 ± 0.21	0.23 ± 0.02	6 ± 3	1.64 ± 0.06
Gi592	0.26 ± 0.01	1.19 ± 0.64	5.35 ± 0.21	0.25 ± 0.03	6 ± 3	1.70 ± 0.07
Gi593	0.32 ± 0.02	2.33 ± 0.75	5.41 ± 0.24	0.28 ± 0.03	6 ± 3	1.79 ± 0.07

110 °C thermoluminescence (TL) peak and the absence of a considerable IRSL (infrared stimulated luminescence) signal highlight the purity of the quartz extract (Hütt et al. 1988; Aitken 1998). The OSL ages were calculated
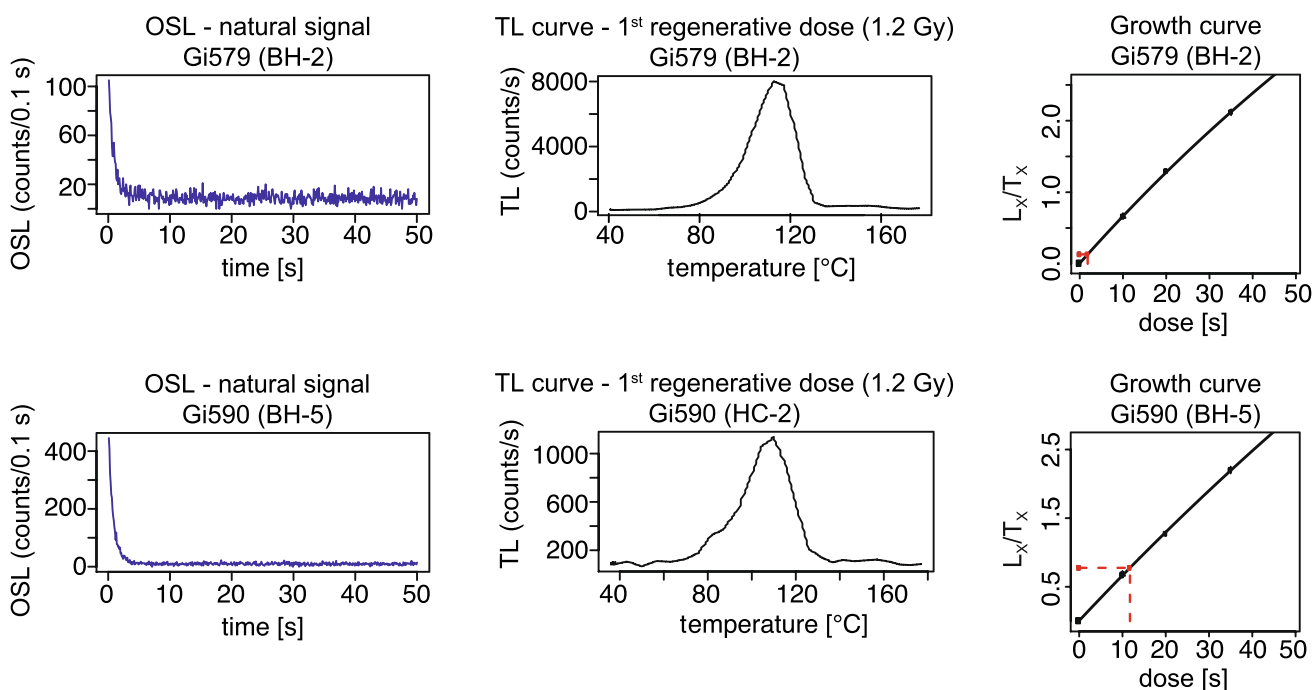
Fig. 9 Luminescence properties of the sediments represented by the samples Gi579 (BH-2) and Gi590 (BH-5). OSL shine-down curves of the natural signal, TL curves of the first regenerated dose preheat and the growth curves are shown. The graphs are created using the function plot_RLum() in the R luminescence package (Kreutzer et al. 2020).

based on the D_e estimates and the parameters listed in Tables 1 and 2. The resulting ages and their 1σ errors are listed in Table 2 and shown in Fig. 4 to 7.

The D_e values were calculated by establishing growth curves with single exponential saturation functions. Based on the resulting D_e distributions and their dispersion parameters (skewness and kurtosis), 11 out of 16 OSL samples were identified as incompletely bleached (Table 2), resulting in the application of the bootstrap minimum age model (Cunningham & Wallinga 2012). The minimum age model was executed with a sigma b value of 0.23, based on the average overdispersion of un-skewed D_e values that were measured for the open-water reservoir at Atar Haroa in the Negev Highlands (Junge et al. 2018). The incompletely bleached samples are often characterized by some outliers with higher doses (e.g., Gi576, Fig. 10). The remaining five samples do not show evidence for insufficient bleaching, and consequently the central age model was used (Galbraith et al. 1999).

The occurrence of incomplete bleaching does not appear to be caused by a certain mode of deposition at this site, because samples considered to be incompletely bleached can be found in all the sections. This includes the fluvial sediment accumulation within the channel and the cistern fill, as well as the retaining wall and spoil pile sediments transported and deposited by humans. For the retaining wall and the spoil pile (BH-3 and BH-5), incomplete bleaching might occur because the sediments were shovelled and moved by humans in large quantities rapidly over a short distance. This can result in insufficient exposure to sunlight, causing residual OSL signals in a portion of the grains. However, fluvial transported sediments accumulated in the channel (BH-1 and BH-2) and cistern (BH-4) sometimes show evidence for incomplete bleaching, as well. In this case, the individual grains are more likely to be exposed to sunlight, but due to the small catchment size, the transport distances are relatively short, reducing the possibility of complete bleaching of all grains. Also, the high-energy rainfall events, typical for this arid environment, generate a high transport capacity resulting in carrying of large amounts of material in short periods of time, hampering the bleaching of the quartz grains. Additionally, the dominant carbonate lithology of the Negev Highlands often results in aggregates or carbonate coatings of the grains, and therefore reduces the likelihood of bleaching individual grains. Finally, one should also consider the possibility of post-depositional mixing by animal burrowing, where sediments from over- or underlying strata could be incorporated into the sampled layer.

The relative standard deviations (RSD) and overdispersions (OD) are fairly high, ranging between 11 to 93% and 9 to 90%, respectively. In general, OD and RSD tend to increase with decreasing D_e values, because the residual doses increase relatively to the dose accumulated since the last bleaching event. Hence, even the smallest residual doses due to incomplete bleaching or the incorporation of grains from other layers can cause wide distributions for low D_e values. For some of the samples from the studied site, the wide distributions are dominantly caused by outliers and can be associated with incomplete bleaching (Fuchs et al. 2007). Besides the high RSD, these samples are also characterized by skewed D_e distributions. But even some samples with un-skewed D_e distributions have higher OD and RSD values (e.g., Gi584: RSD = 32%, OD = 32%, Fig. 10) than expected for a well-bleached sample. An explanation for this might be a heterogeneous microdosimetry (Mayya et al. 2006). Microdosimetric effects can cause an increase of the RSD, especially with lower contents of U, Th and K, like in the case for the studied sediments (Table 1). The carbonatic nature of these deposits (see micromorphology section below) may amplify this effect.

Micromorphology

Sample BH-4-M was collected at the bottom of trench BH-4 within cistern I (Figs. 6 and 11). The lower 5 cm of the sample, reddish-brown in colour, is composed primarily of a micritic calcite groundmass that includes quartz grains (Fig. 11b–d). The microstructure is massive with occasional channels and chambers indicative of bioturbation. Fe/Mn-oxide stains and nodules are present, evidencing hydromorphic conditions. The next unit of sediments (6 cm thick; greyish with brownish patches) is characterized by a more open structure due to the inclusion of chalk gravel (Fig. 11a, e). Angular gravel probably originates from erosion of the cistern walls. Rounded chalk gravel occurs as well, probably originating from washed in debris. Finer components include calcite and quartz grains. The uppermost deposit (3 cm thick; greyish) is composed of rounded chalk gravel and finer grains (calcite and quartz sand), probably all originating from washed in debris.

Sample BH-5-M was collected from the spoil pile of cistern IV covering the transition between pre-construction and construction material in the lowermost step (Figs. 7 and 12). The lower 3–4 cm of the sample (Fig. 12b–d), yellowish-brown in colour, is composed of calcitic clay with abundant quartz silt and sand. The sediment is poorly sorted, including many snail shell fragments and rounded chert gravel. Its upper contact is uneven but sharp. This deposit is interpreted as the palaeosurface. The deposit overlying the palaeosurface (8–9 cm thick; light yellowish) is composed of angular chalk and chert gravel within a calcitic matrix (Fig. 12a, d). Snail shell fragments and quartz grains occur but in small quantities relative to the palaeosurface. This deposit is interpreted as resulting from cistern construction. Its contact with the overlying deposit is sharp. The latter deposit is a thin

Table 2 Sample ID, deposition mode, sampling depth, equivalent dose (D_e), number of measured aliquots, aliquot diameter, overdispersion, relative standard deviation, transformation for D_e calculation (logged or unlogged), used age models (*CAM* central age model, *MAM* minimum age model) and the resulting OSL age.

Sample ID	Section location/deposition mode	Sampling depth [cm]	D_e [Gy]	Number of aliquots	Aliquot diameter [mm]	Overdispersion [%]	Rel. standard deviation [%]	Logged or unlogged	Age model	Age [ka]	Age in calendar years
BH-1	Channel fill										
Gi576	Abandonment	70	0.31±0.05	28	4	90	93	Unlogged	MAM	0.17±0.03	1820–1880 CE
Gi577	Abandonment	20	1.09±0.12	24	3	59	61	Unlogged	MAM	0.66±0.08	1280–1440 CE
BH-2	Channel fill										
Gi578	Abandonment	45	0.38±0.02	27	3	28	29	Unlogged	CAM	0.19±0.01	1820–1840 CE
Gi579	Abandonment	33	0.23±0.04	36	3	82	86	Unlogged	MAM	0.13±0.02	1870–1910 CE
Gi580	Abandonment	17	0.27±0.04	29	3	47	49	Unlogged	MAM	0.16±0.02	1840–1880 CE
BH-3	Retaining wall										
Gi581	Maintenance	33	0.35±0.09	28	4	65	67	Unlogged	MAM	0.19±0.05	1780–1880 CE
Gi582	Maintenance	60	0.58±0.05	29	4	63	65	Unlogged	MAM	0.32±0.03	1670–1730 CE
Gi583	Construction	39	2.04±0.15	31	2	38	39	Unlogged	CAM	1.1±0.1	800–1000 CE
Gi584	Construction	41	2.17±0.15	27	2	32	32	Logged	CAM	1.3±0.1	600–800 CE
BH-4	Cistern fill										
Gi585	Abandonment	182	0.41±0.07	25	4	65	66	Unlogged	MAM	0.27±0.05	1700–1800 CE
BH-5	Spoil pile										
Gi588	Pre-construction	110	21.14±2.49	36	1	37	40	Logged	MAM	9.2±1.1	8300–6100 BCE
Gi589	Construction	70	2.00±0.17	23	2	37	39	Unlogged	CAM	1.6±0.2	200–600 CE
Gi590	Maintenance	30	1.39±0.06	36	2	21	25	Unlogged	MAM	0.87±0.05	1100–1200 CE
Gi591	Construction	41	2.43±0.19	24	2	16	20	Logged	MAM	1.5±0.1	400–600 CE
Gi592	Construction	21	2.43±0.09	23	2	9	11	Logged	CAM	1.5±0.1	400–600 CE
Gi593	Maintenance	8	0.87±0.06	21	3	46	50	Unlogged	MAM	0.49±0.04	1490–1570 CE

Fig. 10 Kernel density estimation plot for representative samples (Gi576, Gi584, Gi588 and Gi589). For these samples, the accepted aliquots are shown in ascending order, with n (number of aliquots), RSD (relative standard deviation), mean D_e (equivalent dose) and the aliquot diameter. The graphs were created with the function plot_KDE() in R using the luminescence package (Kreutzer et al. 2020).
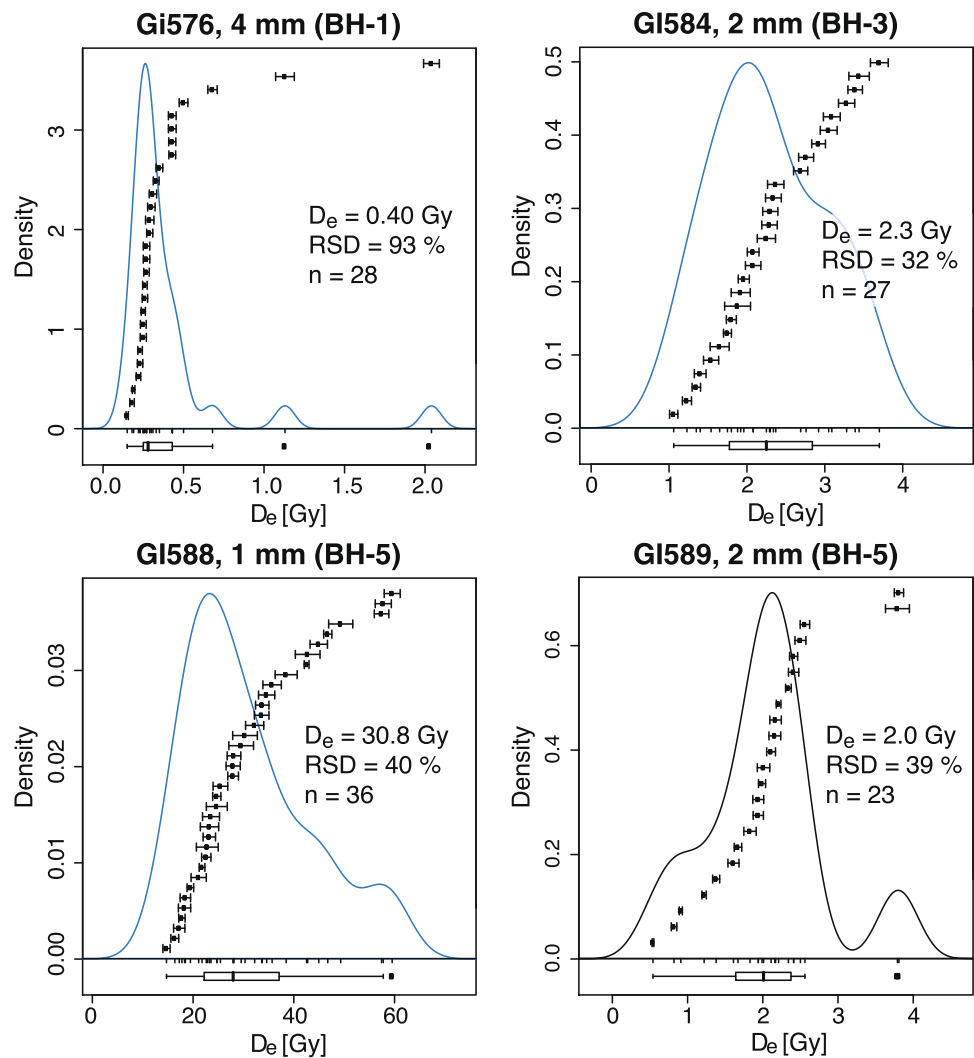
(no more than 1 mm thick) greyish layer of 1–2 micritic calcite crusts that seems to indicate sheetwash (Fig. 12e). This deposit signifies exposure of the deposit below it for at least one winter. The deposit that overlies the crust(s) (2 cm thick) is mostly fine (i.e., no chert or chalk gravel) composed of calcitic clay, with a few snail shell fragments (Fig. 12f). Notably, it includes fragments of crusts, some of them oriented sub-vertically, which are typical for sediment accumulations removed from cisterns.

Discussion

To interpret the OSL results and therefore to reconstruct the cisterns system's history, micromorphological analyses, field stratigraphy and the bleaching abilities for different modes of deposition need to be taken into consideration. This is done separately for the spoil pile of cistern IV and the retaining wall, channel fill and cistern fill of cistern I.

The spoil pile (BH-5) of cistern IV

Above bedrock, four stratigraphic units can be distinguished macroscopically in the bottom step of trench BH-5 (Figs. 7b and 13). The lowermost sediment unit is about 45 cm thick and consists of yellowish-brown calcitic loam with many cobbles (dominantly flint, < 15 cm) and a few boulders. This unsorted alluvial deposit yields an OSL age of 9.2 ± 1.1 ka (Gi588). The deposition of the material during the Early Holocene and the sediment properties clearly marks this layer as natural deposition before the cistern was constructed. These sediments are sharply separated (Fig. 12b) from the overlying ca. 35-cm-thick light yellowish deposits composed of calcic fines with a few flint cobbles (up to 10 cm). Microscopically, it shows a distinctly different composition and microstructure with abundant angular chalk fragments typical of construction deposits (Fig. 12d). The OSL dating of this unit yields an age of 1.6 ± 0.2 ka (Gi589), indicating construction during the late-Roman or Byzantine period. Due to the absence of fine to medium quartz sand

Fig. 11 Micromorphology of deposits within cistern I. **a** Flatbed scan of the thin section of the upper part of the block sample. **b** Flatbed scan of the thin section of the lower part of the block sample. **c** Microphotograph (PPL) of the lower reddish-brown layer. Note vesicles from bioturbation and dark Fe/Mn-oxide nodules from hydromorphic conditions within the cistern. **d** Same as c but under XPL. The fine whitish speckles are from quartz silt and fine sand. **e** Microphotograph of the upper mixed layer of the deposit. Note the open structure with a rectangular fragment of chalk (middle of the image) surrounded by disintegrated chalky matter. Scale bar in **c–e** is 500 μm.
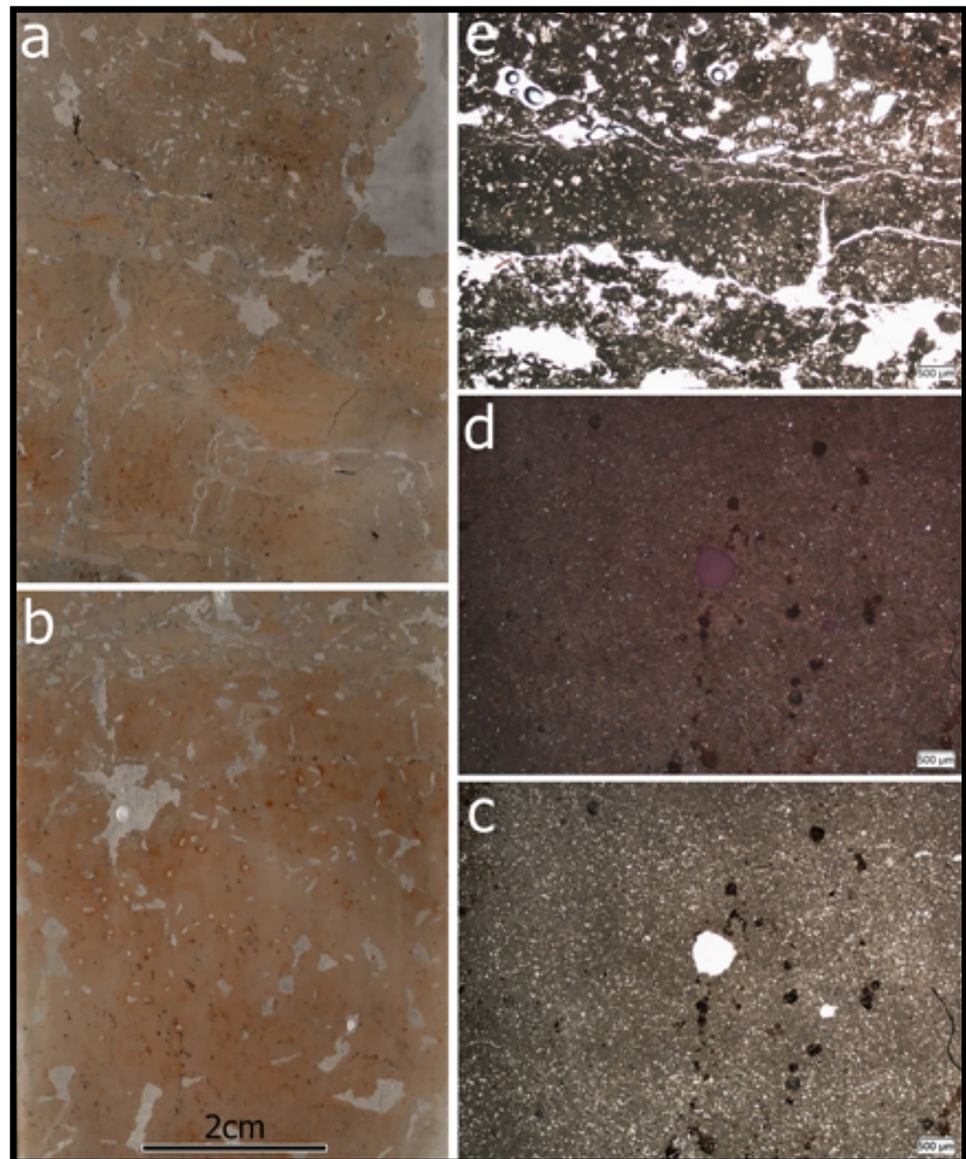
in the chalk bedrock, it is assumed that quartz grains were incorporated into the construction deposit either by humans trampling over the spoil pile or by aeolian transport during the ongoing construction work. The D_e values of the OSL sample Gi589 show a slightly left-skewed distribution with several lower values (Fig. 10). The skewed distribution can be the result of the incorporation of grains with a lower OSL signal or two sample populations, due to separate deposition events. To minimize the risk of post-depositional incorporation of younger grains and to ensure that the sampled grains were incorporated during construction, the dated material was taken from the centre of the construction layer. Accordingly, it is more likely that the high amount of calcium carbonate of the sediment increased the attenuation of the ionizing radiation, especially for grains with a calcium carbonate crust, and the low dose rate ($\dot{D}$ in Table 1) of

the sample caused microdosimetric effects, resulting in a slightly left-skewed distribution. Despite the occurrence of low D_e values, the distribution parameters (Bailey & Arnold 2006) of the sample led to the use of the CAM, putting no stronger emphasis on the low D_e values to prevent an age underestimation.

The upper part of the micromorphology block contains a ca. 1-mm-thick crust marking sheetwash within the construction layer (Fig. 12e). This indicates a time gap of at least one winter of exposure between the two depositions within this unit. The upper part of the micromorphological sample shows crust fragments with various orientations that are typical for sediment refill that was removed from cisterns during maintenance operation. This and the thin crust indicate that the construction of the cistern took place over the course of at least 1 year, with a partial refill of the cistern

Fig. 12 Micromorphology of the spoil pile of cistern IV. **a** Flatbed scan of the thin section of the upper part of the block sample. The arrow indicates the location of in situ crusts (image **e**, see below). **b** Flatbed scan of the thin section of the lower part of the block sample. Arrow indicates the contact between the reddish-brown alluvial deposition and the construction material of the spoil pile. **c** Microphotograph (PPL) of the alluvium. Note abundant transparent rounded quartz particles as well as elongated snail shell fragments. **d** Microphotograph of the coarse fragments typical of the deposit consisting of construction debris. PPL. **e** Microphotograph (PPL) of the finer-grained deposit consisting of two sub-horizontal crusts indicating aerial exposure and sheetwash. **f** Microphotograph (PPL) of the fine-grained deposit consisting of sub-vertical elongated fragments of crusts resulting from cistern maintenance activities. Scale bar in **c–e** is 500 μm.
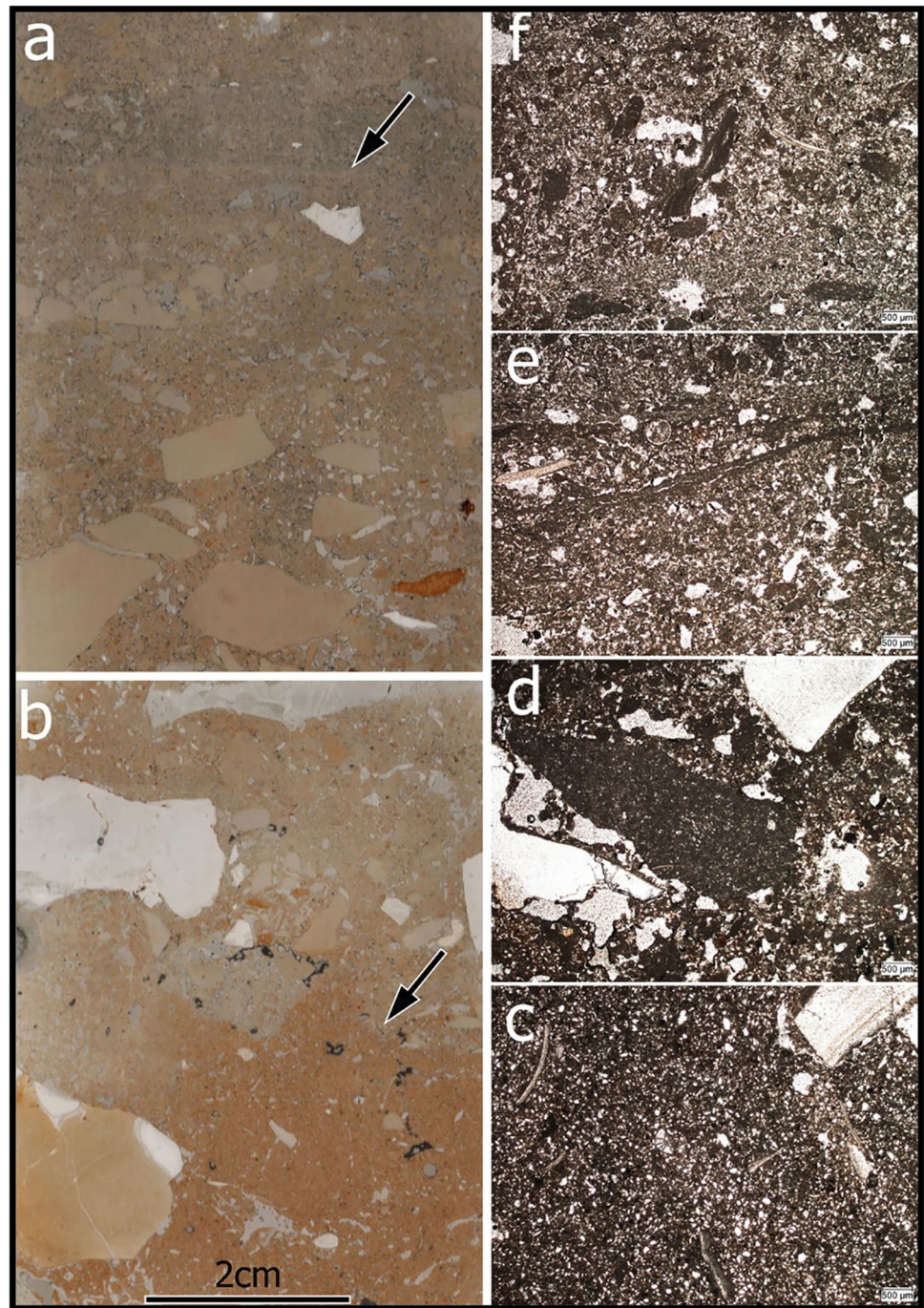
during this time. A temporal resolution of such short time spans is not possible with OSL dating.

The overlying unit in the upper centre of the lower step is characterized by light yellowish calcitic fines with many unoriented chalk cobbles and a few flint cobbles (up to 7 cm). The chalk cobbles indicate construction because they originate from the relocation of bedrock, while the majority of the flint gravels were washed from the slopes into the cistern and then removed in terms of cistern maintenance. The dating of sample Gi590 yields a time of deposition 0.87 ± 0.05 ka ago. The sedimentary properties of the material do not allow a definite distinction of the deposition mode: it is possible that the material was either deposited on top of the spoil pile during the initial construction in the late-Roman or Byzantine period and later washed or tramped down during the twelfth century, or the material was deposited in this location during cistern maintenance during the twelfth century. The thin top layer of the lower step is also composed of weakly compacted, light yellowish sandy silt, but carries only very few small cobbles (< 4 cm).
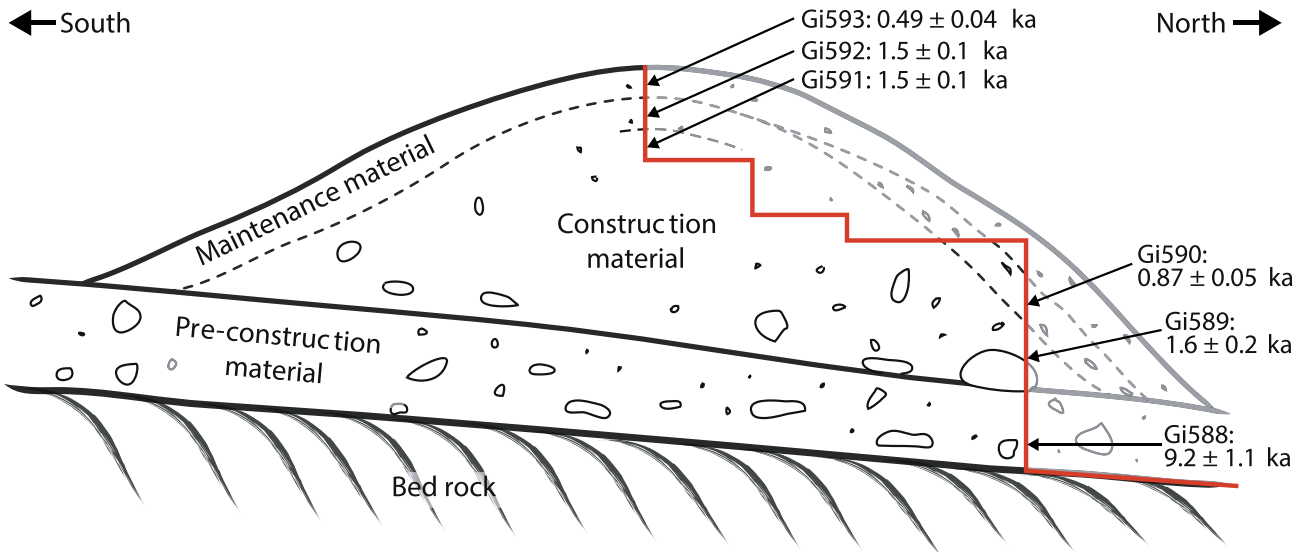
Fig. 13 Schematic section of spoil pile IV (the stepped trench is marked in red), displaying OSL ages and layers observed in the field.
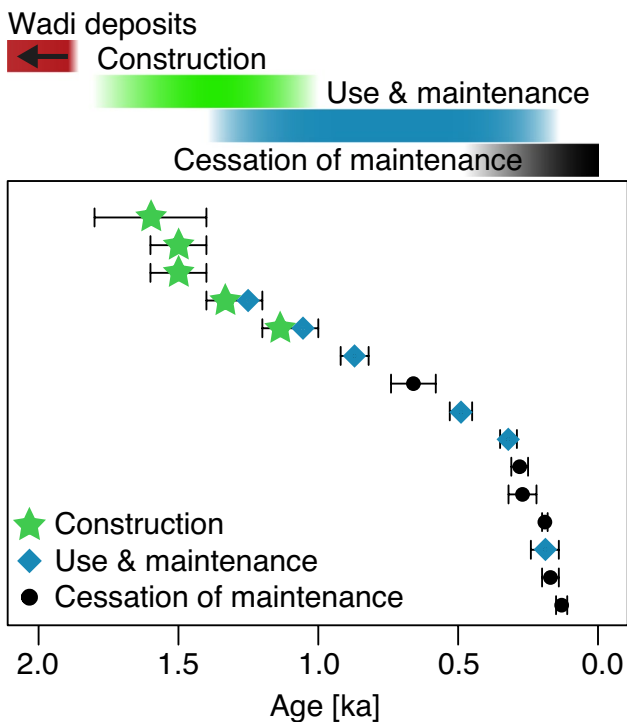
Fig. 14 Summary of the age ranges of the OSL samples ordered in accordance to their age, indicating construction (green), use and maintenance (blue), and the cessation of maintenance (black) of the cistern system. The position of the age of alluvial deposition is only implied, because of its high value. Two of the samples of the retaining wall could not be clearly identified as construction or maintenance; hence, they are marked as both in this graph (green star and diamond).

The material was not sampled for dating due to its proximity to the current surface and the lack of compaction, which risks mixing of the material from the surface with the upper part of the spoil pile.

The upper step of the BH-5 trench (Figs. 7a and 13) is composed of three macroscopically defined units, each 16–18 cm thick. The two lower deposits consist of yellowish fines with very few gravels and are assumed to be relocated bedrock material from the cistern's construction, because of its homogeneous composition and the light colour. The layer in the centre of this section is only distinguished from the lower unit by its slightly stronger compaction. The OSL dating of both units results in the similar age of 1.5 ± 0.1 ka (Gi591 and Gi592). Within their errors, these ages agree with sample Gi589 (1.6 ± 0.2 ka) in the lowest step of the spoil pile trench (Fig. 13), which strengthens the dating of the cistern's construction to the late-Roman to Byzantine period. The two slightly distinguishable layers might reflect the time gap within the construction that is reflected by unoriented fragments of crusts in the micromorphology sample from the lower step (BH-5-M). The consensus of the three samples can be used as an age control showing the reliability of the OSL dating at this site, and that the application of the MAM is able to correct incomplete bleaching (as used for sample Gi591). The uppermost layer of the spoil pile is a slightly compacted yellowish-brown sandy silt with some pebbles and very few stones (< 5 cm, flint). The OSL age of 0.49 ± 0.04 ka and the location on top of the spoil pile marks this unit as maintenance material—possibly the final cleaning of cistern IV.

To summarize, the OSL dating of the spoil pile allows the construction of cistern IV to be constrained to the third to

sixth century CE, during the late Roman or Byzantine periods. One phase of the cistern's maintenance likely occurred during the twelfth century CE, while this age could also reflect a post-depositional transport of construction material from the upper part of the spoil pile. The latest use in terms of maintenance material dates to ca. 1500 CE and marks the earliest possible date for the beginning of the final infill and the subsequent end of cistern IV maintenance.

The retaining wall (BH-3) of cistern I

Trench BH-3 (Fig. 5) exposed material deposited in order to construct and possibly reinforce the retaining wall diverting water into cistern I. The channel-facing side of the retaining wall is constructed of flat stones. On top of the piled stones, and in the centre and lower end of the retaining wall, yellowish sandy silt, many cobbles in different sizes and some boulders (up to 50 cm) accumulated. No layering or changes in the sediment composition throughout the trench could be identified. The two lower samples Gi584 and Gi583 yield ages of 1.3 ± 0.1 ka and 1.1 ± 0.1 ka, respectively (late Byzantine and early Islamic periods), and therefore are the same within their 2σ errors. To interpret these ages, it is essential to understand that only a limited amount of water would reach the cistern without the retaining wall. Consequently, it is assumed that the retaining wall was constructed contemporaneously with the cistern or shortly thereafter. However, the stacked stone pile can be interpreted as the initial retaining wall that was extended and enhanced by unsorted sediments either at the time of construction or at a later stage. Since the deposition of the piled stones was not dated directly, it is not clear if the ages of samples Gi584 and Gi853 represent the initial construction of the retaining wall or its later extension. Therefore, these OSL results should be interpreted as the latest possible ages for the construction of the retaining wall and consequently the cutting of cistern I.

The two upper OSL samples provide ages of 0.32 ± 0.03 ka (Gi582) and 0.19 ± 0.05 ka (Gi581), respectively. Within 2σ errors, the two ages agree with each other. Because no sediment layering was observed, it can be assumed that the sediments were deposited during a single event, although multiple events within the OSL age range cannot be excluded. In any event, these ages indicate that the retaining wall was heightened during the seventeenth to the nineteenth century with material possibly originating from maintenance material from the cistern and the adjacent channel.

To summarize, two deposition events can be distinguished: the older OSL ages are assumed to represent the minimum age of the construction of the retaining wall, and possibly of the construction of the associated cistern I, during the late Byzantine to Early Islamic period or earlier. The younger OSL ages represent a deposition during the seventeenth to the nineteenth century and might reflect the enhancement of the retaining wall, or the cleaning of cistern I and its channel.

The channel fill (BH-1 and BH-2)

Trenches BH-1 and BH-2 were cut into the sediment deposition within a channel directing water into cistern I (Fig. 4). The bottom of both is bounded by bedrock. The overlying sediment is composed of alternating layers of sandy silts and gravels with a few stones (< 15 cm), indicating depositional events of varying magnitude. While the sandy silt layers are interpreted as fluvial deposits, the deposits with larger gravels and stones may be understood as gravitational transported slope debris.

The OSL samples from trench BH-2 yield ages of 0.19 ± 0.01 ka (Gi578), 0.13 ± 0.02 ka (Gi579) and 0.16 ± 0.02 ka (Gi580), while the bottom sample in trench BH-1 yields an age of 0.17 ± 0.03 ka (Gi576). Considering their 2σ errors, all ages are the same, indicating that sediment accumulation in the channel occurred during the nineteenth century. The uppermost sample in trench BH-1 yields an age of 0.66 ± 0.08 ka (Gi577), resulting in an age inversion in the trench. This age overestimation can be explained by poor exposure to sunlight during the sediment transport, e.g., turbid water over short transport distances within short time periods, or transport and deposition during the night. Besides Gi577, samples Gi576, Gi579 and Gi580 also show D_e distributions with characteristics of incomplete bleaching. The application of the MAM for the three samples (Gi576, Gi579 and Gi580) results in the agreement of the ages with the results from the well-bleached sample (Gi578). The use of the MAM for sample Gi577 still results in a strong overestimation of the age. This can be caused by no grains or only very few grains being bleached during transport. When only a few well-bleached grains are mixed with a high number of grains with residual doses, no measured aliquot represents the final transport and deposition, but rather earlier bleaching events. In other words, the MAM emphasizes aliquots with lower doses, but these still overestimate the time of the final deposition. Thus, it is impossible to interpret the age of sample Gi577.

The younger ages obtained from BH-1 and BH-2 point to sediment accumulation after the last cleaning of the channel during the nineteenth century. This latest accumulation within the channel corresponds with the sediment deposition on the retaining wall (BH-3: Gi581 and Gi582, ca. late seventeenth to early nineteenth century CE).

Cistern fill (BH-4)

The sediments within cistern I (BH-4, Fig. 6) are composed of sandy silt with some gravels (< 1 cm) and a few stones (< 20 cm), two sandy layers in the lower part and two shallow organic-rich layers near the top. The stones within the trench most likely fell through the partially collapsed roof of the cistern from the adjacent slope, or are parts of the roof collapse. It is unlikely that stones of this size were washed into the cistern by surface runoff from the channel, because the water and sediments in the channel are slowed by the retaining wall and the reduced transport capacity of the runoff water hampers the further transport of larger stones into the cistern. This assumption is supported by the limited number of gravels and other stones in the layers where the large stones occur. The bottom of the cistern was not reached; excavation was stopped when an enamelled metal bucket (twentieth century) was exposed at a depth of 180 to 200 cm. The material at this depth was compacted due to the overburden in a moist environment, as it can be seen in the bottom part of the micromorphology sample (Figs. 11b–d). The OSL dating at this depth results in an age of 0.27 ± 0.05 ka (Gi585), indicating the last maintenance within cistern I probably took place no later than the eighteenth century. In comparison to OSL ages from BH-1 and BH-2, this would mean that the channel of cistern I was still cleaned for one or two centuries when the cistern itself was no longer maintained. This scenario cannot be ruled out, because the shallow channel is filled with sediments more rapidly than the cistern; thus, the cistern needs to be maintained less often. At the same time, the appearance of plastic and metal trash deep in the trench indicates a very recent sediment accumulation. While this is in accordance with the information shared by a local farmer about cleaning activities in cistern III in the 1960s by members of a nearby kibbutz, it is assumed that Bedouin have been using these cisterns until recently as well. This recent maintenance might have been also carried out in cistern I, hinting towards later utilization. The discrepancy between the OSL age and the stratigraphic evidence in this section indicates that insufficient bleaching occurred that cannot be corrected by the application of the MAM. The reasons for this are similar to the causes of the age overestimation of sample Gi577 in BH-1.

Bleaching

During construction and maintenance, large amounts of material were removed by humans and transported over a very short distance to the spoil pile. Despite the unfavourable conditions for bleaching, the results show that incomplete bleaching is an issue only for one of the construction samples (Gi591). For this sample, the age agreement with other samples from the same event shows the successful application of the MAM to correct for the age overestimation due to residual signals on some of the quartz grains. This better than expected bleaching of the construction material may result from the fact that the quartz grains do not originate from the hewn chalk bedrock, but from dust incorporated either naturally or by humans walking over the spoil pile during ongoing construction work. The long exposure of the spoil pile layers during construction, due to slow construction of the cisterns, supports the bleaching of the incorporated grains.

While the construction material was transported and deposited once, the sediments removed during cleaning were moved twice: first, when they washed into the cisterns and channels, and second, when they were removed from the installations during maintenance. Despite this, all maintenance samples from the site suffer from broad, skewed distributions indicating insufficient bleaching. The resetting of the OSL signal during the fluvial transport often suffers from incomplete bleaching as evidenced by the samples from the sediment accumulations within the channel and cistern. This poor bleaching might be the result of the short transport distances, large amounts of material transported, water turbidity, or a transport and deposition event overnight. This might be amplified by the transport of sediments that accumulated initially in the catchment during the Late Pleistocene or Early Holocene, resulting in an even older OSL signal to be reset. The second transportation and deposition of the maintenance material was carried out by humans. Other than the construction material, the infill sediments were likely unconsolidated and easy to remove from the installations, which potentially made this process faster and limited the exposure of sediments on top of the spoil pile to sunlight, reducing bleaching time.

Furthermore, the younger ages of the maintenance material in general and the final accumulation within the installations in particular are more vulnerable to residual doses, because the dose accumulated since the last deposition is quite small. This can result in considerable age overestimations even with very minor residual doses. For most of the samples, this issue is controllable with the application of MAM, but if no or only very poor bleaching occurs, the MAM still results in an age overestimation, as in the case for the samples Gi577 and Gi585. In these cases, it is necessary to compare them with other samples from the same or similar units and to put them in a stratigraphical context. The handling of the incomplete bleaching as described here, and the incorporation of micromorphological analyses for the interpretation of the mode of deposition, allows the establishment of a chronology of the cistern system at Borot Hazaz.

Overall chronology of the Borot Hazaz cistern system

As described above, the chronology of subterranean cisterns in the Negev Highlands is based on hypotheses regarding architectural similarities, proximity and a handful of inscriptions. This has resulted in an assumption that construction of rock-cut cisterns took place only during the Hellenistic-Roman (Nabatean) to Byzantine Period. The use of OSL allows the dating of sediment transported during construction and cleaning (maintenance) of the cisterns, as well as fluvial sediment accumulation in the installations when maintenance declines or ceases. For cistern IV, the archaeological age assessment is supported by OSL dating, indicating construction during the Late Roman to Byzantine Period. For cistern I, the latest possible date of construction is 600–1000 CE (Late Byzantine to Early Islamic periods). A possible maintenance phase for cistern IV took place during the twelfth century and final maintenance of this cistern is dated to the fifteenth to the sixteenth century. In comparison, cistern I was maintained and utilized at least until the seventeenth to the nineteenth century. These data indicate that the Borot Hazaz cisterns may have been constructed at slightly different times and not as a complete system in one campaign. Additionally, the cisterns studied here were used and maintained differently.

The Byzantine period features unprecedented prosperity in the Negev Highland, with several urban centres and a large number of smaller settlements and farmhouses, being the only period in the history of the Negev Highlands which also supplies textual evidence for agricultural activity (Rubin 1988; Tepper et al. 2020). Scholars debate whether this activity declined relatively abruptly at the end of the Byzantine period (recently Tepper et al. 2018), or gradually during the Early Islamic period (Haiman 1995; Avni 2008, 2014). The study at Borot Hazaz is too limited to shed light on this issue. However, together with a previous study on an open-water reservoir located nearby (Junge et al. 2018), it is shown that cisterns were utilized and maintained by (agro) pastoral groups in the region for centuries after the decline of the Byzantine settlement system.

Conclusion

The dating of the cisterns system of Borot Hazaz benefits from the very suitable characteristics of the coarse-grain quartz fraction for OSL dating. Despite the unfavourable bleaching conditions of short transport distances, the majority of samples were well-bleached. Of the samples insufficiently bleached, the application of the MAM was able to successfully correct for the age overestimation, as confirmed by the agreement of the resulting ages with other OSL ages from associated sediments and events. Only for two samples, the comparison with other ages or the sedimentary context reveals an age overestimation that cannot be corrected. Overall, the interpretation of the OSL ages is supported and enhanced by the micromorphological analyses. The identification of different modes of deposition is necessary to distinguish between sediment accumulation before and during cistern construction, and to differentiate material deposited when the installation was maintained, and sediment accumulation after maintenance ceased.

The combination of OSL dating and micromorphology confirms the archaeological age assessment of cistern IV: construction took place during the late Roman to Byzantine Period. For cistern I, construction can only be given as a minimum age—before or during the Early Islamic Period. A maintenance phase of cistern IV took place during the twelfth century and final maintenance for this cistern was conducted during the fifteenth to the sixteenth centuries. For cistern I, later maintenance and utilization can be dated to the seventeenth to the nineteenth century. It is notable that there are substantial time gaps between the construction phases and the maintenance of the installations, and that the different cisterns of the system were likely constructed and used at different times.

References

Aitken MJ (1998) An introduction to optical dating. Oxford University Press, Oxford

Arnold LJ, Roberts RG, Galbraith RF, DeLong SB (2009) A revised burial dose estimation procedure for optical dating of young and modern-age sediments. Quat Geochronol 4:306–325

Avni G (2008) The Byzantine-Islamic transition in the Negev: an archaeological perspective. Jerus Stud Arab Islam 35:1–26

Avni G (2014) The Byzantine–islamic Transition in Palestine: an Archaeological Approach. Oxford University Press, Oxford

Avni Y, Weiler N (2013) Geological map of Israel 1:50,000: Sede Boqer sheet 18-IV. Jerusalem, Israel: Ministry of Energy and Water Resources, Earth and Marine Research Administration, Geological Survey.

Avni Y, Porat N, Plakht J, Avni G (2006) Geomorphic changes leading to natural desertification versus anthropogenic land conservation in an arid environment, the Negev Highlands. Israel Geomorphology 82(3–4):177–200

Avni Y, Porat N, Avni G (2012) Pre-farming environment and OSL chronology in the Negev Highlands, Israel. J Arid Environ 86:12–27

Avni G, Porat N, Avni Y (2013) Byzantine—Early Islamic agricultural systems in the Negev Highlands: Stages of development as interpreted through OSL dating. J Field Archaeol 38(4):332–346

Bailey RM, Arnold LJ (2006) Statistical modelling of single grain quartz De distributions and an assessment of procedures for estimating burial dose. Quatern Sci Rev 25(19–20):2475–2502

Bailey RM, Smith BW, Rhodes EJ (1997) Partial bleaching and the decay form characteristics of Quartz OSL. Radiat Meas 27(2):123–136

Bar-Matthews M, Ayalon A, Gilmour M, Matthews A, Hawkesworth CJ (2003) Sea–land oxygen isotopic relationships from planktonic Foraminifera and speleothems in the Eastern Mediterranean region and their implication for paleorainfall during interglacial intervals. Geochim Cosmochim Acta 67(17):3181–3199

Bar-Matthews M, Ayalon A (2004) Speleothems as palaeoclimate indicators, a case study from Soreq Cave located in the eastern Mediterranean region, Israel. In: Battarbee RW, Gasse F, Stickley CE (eds) Past climate variability through Europe and Africa. Springer, Dordrecht, Netherlands, pp 363–391

Boaretto E, Finkelstein I, Shahack-Gross R (2010) Radiocarbon results from the Iron IIA site of Atar Haroa in the Negev Highlands and their archaeological and historical implications. Radiocarbon 52:1–12

Bookman R, Enzel Y, Agnon A, Stein M (2004) LateHolocene lake levels of the Dead Sea. Bulletin of the Geological Society of America 116:555–571

Bowman D, Karnieli A, Issar A, Bruins HJ (1986) Residual colluvioaeolian aprons in the Negev Highlands (Israel) as a paleo-climatic indicator. Palaeogeogr Palaeoclimatol Palaeoecol 56:89–101

Bruins HJ (1986) Desert environment and agriculture in the Central Negev and Kadesh Barnea during historical times (Published PhD dissertation). University of Wageningen, Wageningen, the Netherlands, Stichting Midbar Foundation, Nijkerk, the Netherlands

Bruins HJ (2012) Ancient desert agriculture in the Negev and climate-zone boundary changes during average, wet and drought years. J Arid Environ 86:28–42

Burow C (2020) calc_AliquotSize(): Estimate the amount of grains on an aliquot. Function version 0.31. In: Kreutzer, S., Burow, C., Dietze, M., Fuchs, M.C., Schmidt, C., Fischer, M., Friedrich, J., 2020. Luminescence: Comprehensive Luminescence Dating Data Analysis. R package version 0.9.8.9000–72. https://CRAN.R-project.org/package=Luminescence.

Cohen R (1981) Survey of Sede Boqer Southwest – Map 168. Jerusalem.

Cohen R, Cohen-Amin R (2004) Ancient settlement of the Negev Highlands: the Iron Age and the Persian period (Vol. II, in Hebrew). Jerusalem, Israel: Israel Antiquities Authority.

Crouvi O, Amit R, Enzel Y, Porat N, Sandler A (2008) Sand dunes as a major proximal dust source for Late Pleistocene loess in the Negev Desert. Israel Quaternary Research 70(2):275–282

Cunningham AC, Wallinga J (2012) Realizing the potential of fluvial archives using robust OSL chronologies. Quat Geochronol 12:98–106

Duller GAT (2003) Distinguishing quartz and feldspar in single grain luminescence measurements. Radiat Meas 37:161–165

Dunseth ZC, Junge A, Lomax J, Boaretto E, Finkelstein I, Fuchs M, Shahack-Gross R (2017) Dating archaeological sites in an arid environment: a multi-method case study in the Negev Highlands, Israel. J Arid Environ 144:156–169

Durcan JA, King GE, Duller GAT (2015) DRAC: dose rate and age calculator for trapped charge dating. Quat Geochronol 28:54–61

Evenari M, Aharoni Y, Shanan L, Tadmor NH (1958) The ancient desert agriculture of the Negev: III. Early Beginnings Israel Exploration Journal 8(4):231–268

Evenari M, Shanan L, Tadmor N (1982) The Negev: the challenge of a desert, 2nd edn. Harvard University Press, Cambridge, MA

Faershtein G, Porat N, Avni Y, Matmon A (2016) Aggradation–incision transition in arid environments at the end of the Pleistocene: an example from the Negev Highlands, southern Israel. Geomorphology 253:289–304

Fuchs M, Wagner GA (2003) Optical dating of sediments: recognition of insufficient bleaching by small aliquots of quartz for reconstructing soil erosion in Greece. Quatern Sci Rev 22:1161–1167

Fuchs M, Woda C, Bürkert A (2007) Chronostratigraphy of a sedimentary record from the Hajar mountain range, N-Oman. Quat Geochronol 2:202–207

Galbraith RF, Roberts RG, Laslett GM, Yoshide H, Olley JM (1999) Optical dating of single and multiple grains of quartz from Jinmium Rock Shelter, Northern Australia: Part I, experimental design and statistical models. Archaeometry 41(2):339–364

Goldreich Y (2003) The climate of Israel: observation, research and application. Kluwer Academic/Plenum Publishers, New York, NY

Guérin G, Mercier N, Adamiec G (2011) Dose-rate conversion factors: update. Ancient TL 29:5–8

Haiman M (1991) Archaeological survey of Israel, map of Mizpe Ramon Southwest (200). Jerusalem, Israel: Israel Antiquities Authority.

Haiman M (1995) Agriculture and nomad-state relations in the Byzantine and Early Islamic periods. Bull Am Sch Orient Res 297:29–53

Heim C, Nowaczyk NR, Negendank JFW, Leroy SAG, Ben-Avraham Z (1997) Near East desertification: Evidence from the Dead Sea. Naturwissenschaften 84:398–401

Huntley DJ, Godfrey-Smith DI, Haskell EH (1991) Light-induced emission spectra from some quartz and feldspars. International Journal of Radiation Applications and Instrumentation. Part D. Nuclear Tracks and Radiation Measurements 18(1–2):127–131

Hütt G, Jaek I, Tchonka J (1988) Optical dating: K-feldspars optical response stimulation spectra. Quatern Sci Rev 7:381–385

Itzhaki Y (1971) The geological history of the Negev. In: Evenari M, Shanan L, Tadmor NH (eds) The Negev, the challenge of a desert. Cambridge, MA: Harvard University Press.

Junge A, Lomax J, Shahack-Gross R, Dunseth ZC, Finkelstein I, Fuchs M (2016) OSL age determination of archaeological structures using trapped aeolian sediments: A case study from the Negev Highlands, Israel. Geoarchaeology 31:550–563

Junge A, Lomax J, Shahack-Gross R, Finkelstein I, Fuchs M (2018) Chronology of an ancient water reservoir and the history of human activity in the Negev Highlands, Israel. Geoarchaeology 33:695–707

Kafle HK, Bruins HJ (2009) Climatic trends in Israel 1970–2002: warmer and increasing aridity inland. Clim Change 96(1–2):63–77

Kidron GJ (1999) Altitude dependent dew and fog in the Negev Desert. Israel Agricultural and Forest Meteorology 96(1–3):1–8

Kreutzer S, Burow C, Dietze M, Fuchs M, Schmidt C, Fischer M, Friedrich J (2020) Luminescence: comprehensive luminescence dating data analysis. R package version 0.9.7: https://CRAN.R-project.org/package=Luminescence.

Lender Y (1990). Archaeological Survey of Israel, map of Har Nafha (196). Jerusalem, Israel: Israel Antiquities Authority.

Lomax J, Kreutzer S, Fuchs M (2014) Performance tests using the Lexsyg luminescence reader. Geochronometria 41(4):327–333

Lomax J, Mittelstraß D, Kreutzer S, Fuchs M (2015) OSL, TL and IRSL emission spectra of sedimentary quartz and feldspar samples. Radiat Meas 81:251–256

Mayya YS, Morthekai P, MurariMadhav K, Singhvi AK (2006) Towards quantifying beta microdosimetric effects in single-grain quartz dose distribution. Radiation Measurement 41:1032–1039

Mejdahl V (1979) Thermoluminescence dating: beta-dose attenuation in quartz grains. Archaeometry 21:61–72

Migowski C, Stein M, Prasad S, Negendank JF, Agnon A (2006) Holocene climate variability and cultural evolution in the Near East from the Dead Sea sedimentary record. Quatern Res 66(3):421–431

Murray AS, Wintle AG (2000) Luminescence dating of quartz using an improved single-aliquot regenerative-dose protocol. Radiat Meas 32(1):57–73

Murray AS, Wintle AG (2003) The single aliquot regenerative dose protocol: potential for improvements in reliability. Radiat Meas 37:377–381

Neumann FH, Kagan EJ, Leroy SAG, Baruch U (2010) Vegetation history and climate fluctuations on a transect along the Dead Sea west shore and their impact on past societies over the last 3500 years. J Arid Environ 74:756–764

Ore G, Bruins, HJ, Meir IA (2020) Ancient cisterns in the Negev Highlands: types and spatial correlation with Bronze and Iron Age sites. Journal of Archaeological Science: Reports: 30https://doi.org/10.1016/j.jasrep.2020.102227

Orland IJ, Bar-Matthews M, Kita NT, Ayalon A, Matthews A, Valley JW (2009) Climate deterioration in the Eastern Mediterranean as revealed by ion microprobe analysis of a speleothem that grew from 2.2 to 0.9 ka in Soreq Cave. Israel Quaternary Research 71:27–35

Porat N, Rosen SA, Avni Y, Boaretto E (2006) Dating the Ramat Saharonim late neolithic desert cult site. J Archaeol Sci 33:1341–1355

Prescott JR, Hutton JT (1994) Cosmic ray contributions to dose rates for luminescence and ESR dating: large depths and long-term time variations. Radiat Meas 23(2–3):497–500

Roskin J, Tsoar H, Porat N, Blumberg DG (2011) Palaeoclimate interpretations of Late Pleistocene vegetated linear dune mobilization episodes: Evidence from the northwestern Negev dunefield. Israel Quaternary Science Reviews 30(23–24):3364–3380

Rubin R (1988) Water conservation methods in Israel's Negev desert in late antiquity. J Hist Geogr 14:229–244

Shanan L (2000) Runoff, erosion, and the sustainability of ancient irrigation systems in the Central Negev Desert. In: Hassan MA, Slaymaker O (eds) The hydrology-geomorphology interface: rainfall, floods, sedimentation, land use. IAHS Publications, Jerusalem, Israel, pp 75–106

Starinsky A, Zilberman E, Braun M, Sneh A (2010) Geological map of Israel 1:50,000: Revivim sheet 18-II. Jerusalem: State of Israel, Ministry of National Infrastructure, Geological Survey.

Stoops G (2003) Guidelines for analysis and description of soil and regolith thin sections. Soil Science Society of America, Madison, WI

Survey of Israel (2007) Mapping and GIS. Retrieved from https://www.govmap.gov.il.

Tepper Y, Erickson-Gini T, Farhi Y, Bar Oz G (2018) Probing the Byzantine/Early Islamic transition in the Negev: the renewed Shivta excavations, 2015–2016. Tel Aviv 45:120–152

Tepper Y, Porat N, Bar-Oz G (2020) Sustainable farming in the Roman-Byzantine period: dating an advanced agriculture system near the site of Shivta, Negev Desert, Israel. Journal of Arid Environments 177https://doi.org/10.1016/j.jaridenv.2020.104134